

# Test of Analysis Method for Top-Antitop Production and Decay Events

BY R. H. DALITZ<sup>1</sup> AND GARY R. GOLDSTEIN<sup>2</sup>

1. *Department of Physics (Theoretical Physics) University of Oxford*  
*1 Keble Road, Oxford OX1 3NP UK*  
*and*
2. *Department of Physics Tufts University Medford, MA 02155 USA*

We have carried out Monte Carlo calculations on two sets of randomly generated QCD events due to  $p\bar{p} \rightarrow t\bar{t}$  with top mass  $m_t = 170$  GeV, one set leading to  $e^+e^-$  or  $e^\pm\mu^\mp$  or  $\mu^+\mu^-$  2jets (dilepton) and the other leading to  $e^\pm$  or  $\mu^\pm$  4jets (unilepton) configurations, in order to test the likelihood methods we have proposed for determining the top mass by analyses of these two sets of configurations. For the set of unilepton events, our method gives a very efficient and quite sharp measure of the top mass lying several GeV below the input mass. For the dilepton set, our method gives a much broader and markedly asymmetric distribution for the top mass estimates, 75% of them lying below 170 GeV, but the dilepton data will have much lower background than unilepton data. We then illustrate these methods by applying them to the data available from CDF in 1995 and discuss the results obtained in relation to the results for the sets of Monte Carlo events. The dilepton events yield masses spread widely, over 140 to 180 GeV, generally lower than the unilepton events, which cluster around  $175 \pm 8$  GeV. In an appendix, we discuss the nature of the additional “slow”  $\mu^+$  observed in one CDF dilepton event, concluding that it is most probably a “tertiary lepton” resulting from the decay sequence  $b \rightarrow c + \text{hadrons}$ , followed by  $c \rightarrow s\mu^+\nu$ .

## 1. INTRODUCTION

A major step forward in research on the top quark has recently been achieved by the CDF Collaboration (Abe *et al.* 1994a, 1995a,b) and the D0 Collaboration (Abachi *et al.* 1995). Both groups present evidence for the discovery in events interpreted as being due to the following production and decay sequences, observed in experiments with the Tevatron at the Fermi National Accelerator Laboratory at Batavia (Illinois):

$$\bar{p} + p \rightarrow \bar{t} + t + \text{other hadrons}, \quad (1.1)$$

which, according to our theoretical picture of the proton, is initiated, at the subnuclear level, mainly by the quark-antiquark annihilation reaction,

$$\bar{q} + q \rightarrow \bar{t} + t, \quad (1.2)$$

where  $q$  denotes a valence quark,  $u$  or  $d$ , in the proton. This is followed by the rapid decay processes for the top and antitop quarks (lifetime width  $\simeq 1.4$  GeV),

$$t \rightarrow W^+ b \quad \text{and} \quad \bar{t} \rightarrow W^- \bar{b} \quad (1.3)$$

with

$$(a) \quad W^+ \rightarrow l^+ \nu_l \quad \text{or} \quad (b) \quad W^+ \rightarrow u \bar{d} \text{ or } c \bar{s} \quad (1.4)$$

and

$$(a) \quad W^- \rightarrow l^- \bar{\nu}_l \quad \text{or} \quad (b) \quad W^- \rightarrow d \bar{u} \text{ or } s \bar{c}. \quad (1.5)$$

For the  $W^+$  (or  $W^-$ ) decays, the hadronic modes (1.4b) (or (1.5b)) have a net rate of about 9 times the rate for each leptonic mode. It is therefore not surprising that the bulk of the present evidence on the top quark arises from the unilepton events,

$$t\bar{t} \rightarrow b\bar{b}(\bar{q}q)l\nu_l \quad (1.6)$$

rather than from the dilepton events

$$t\bar{t} \rightarrow b\bar{b}l\bar{l}\nu_l\bar{\nu}_l, \quad (1.7)$$

where  $l\bar{l} = (e^+e^-)$ ,  $(e^\pm\mu^\mp)$ , and  $(\mu^+\mu^-)$ . Events of the type

$$t\bar{t} \rightarrow b\bar{b}(\bar{q}q)(\bar{q}q) \quad (1.8)$$

are dominant, of course, but they lead to six final jets, a complicated final state to unscramble, which we do not discuss in this paper: however, see Benlloch, Wainer and Giele (1993) for an optimistic assessment of the latter. A preliminary result has been given by Abe, *et al.* (1997).

Both groups have put forward estimates of  $m_t$ , the top quark mass, on the basis of their own data. The official best estimate (Particle Data Group 1996) is

$$m_t = 180 \pm 12 \text{ GeV}, \quad (1.9)$$

this value being dominated by the CDF result. Updated estimates for  $m_t$  were given by both groups at the recent 18th International Electron-Photon Conference held in Hamburg (Giromini 1997), as follows:

$$(a) \text{ CDF } m_t = 176.8 \pm 6.5 \text{ GeV}, \quad (b) \text{ D0 } m_t = 173.3 \pm 8.4 \text{ GeV}. \quad (1.10)$$

Over several years, we (Dalitz & Goldstein 1992a,b,1994 and Goldstein, Sliwa & Dalitz 1993) and K. Kondo (Kondo 1988,1991, and Kondo, Chikamatsu & Kim 1993) independently, have developed a method for determining whether events of the type reported by CDF and D0 Collaborations are consistent with the hypothesis that they are examples of top-antitop pair creation and their decay through the steps (1.3), (1.4) and (1.5) given above, leading to final states (1.6) and (1.7).

The procedure is to take the measured configuration of momenta for the final leptons and jets in a single event  $i$  and to evaluate the probability  $P_i(m) = P(\text{configuration event } i|m)$  that these production and decay processes could produce the observed configuration if the top quark mass were  $m$ . This evaluation must take into account each step in the processes (1.1) through (1.5).

(a) The initial partons  $q$  and  $\bar{q}$  have momenta  $x\mathbf{P}$  and  $-\bar{x}\mathbf{P}$ , where  $\mathbf{P}$  denotes the incident proton momentum in the proton-antiproton rest-frame. The values  $(x, \bar{x})$  for  $t\bar{t}$  production at the Tevatron are so large (Dalitz & Goldstein

1992b,1994) that  $q$  and  $\bar{q}$  are dominantly valence quarks. The proton structure function  $F(x)$  for valence quarks is well-known in the regime which is important for the process (1.2); the antiproton structure function is  $\bar{F}(\bar{x}) = F(x)$ .

(b) The complete  $(t\bar{t})$  system and its final states are to be viewed in the  $(t\bar{t})$  rest-frame achieved by a suitable boost along  $\mathbf{P}$ . The amplitude for process (1.2) will depend on the angle  $\theta$  between the  $t$ -momentum in this rest-frame and the direction  $\mathbf{P}$  and on the total rest energy  $m(t\bar{t})$  of the  $t\bar{t}$ -system produced. With Quantum Chromodynamics (QCD), this amplitude is usually taken to be that produced by the simplest QCD graph, here that for  $q\bar{q} \rightarrow g \rightarrow t\bar{t}$ , and we have adopted this in our work. We note that this mechanism implies a strong spin-spin correlation between  $t$  and  $\bar{t}$ . For subsequent decays, the angles for various decay products will be defined relative to the plane defined by the  $t\bar{t}$  production plane in the lab frame.

(c) The decay  $t \rightarrow bW^+$  is specified in the  $t$  rest-frame, by angles  $\theta_W^+$  and  $\phi_W^+$ .  $\theta_W^+$  is the angle between the momentum  $\mathbf{p}_{W^+}$  in this frame and the boost direction  $\mathbf{z}_t$  from the  $t\bar{t}$  rest-frame to this  $t$  rest-frame.  $\phi_W^+$  is the azimuth angle of  $\mathbf{p}_{W^+}$  relative to the production plane and the  $\mathbf{z}_t$  axis. Similarly, to specify  $\bar{t} \rightarrow bW^-$ , there are corresponding angles  $\theta_W^-$  and  $\phi_W^-$ . With  $\mathbf{z}_{\bar{t}}$  being the boost direction from the  $t\bar{t}$  rest-frame to the  $\bar{t}$  rest-frame,  $\theta_W^-$  is the angle between the momentum  $\mathbf{p}_{W^-}$  and  $\mathbf{z}_{\bar{t}}$ , while  $\phi_W^-$  is the azimuth angle of  $\mathbf{p}_{W^-}$  relative to the production plane and the  $\mathbf{z}_{\bar{t}}$  axis.

(d) The decay  $W^+ \rightarrow l^+\nu_l$  is specified in the  $W^+$  rest-frame by angles  $\theta_l^+$  and  $\phi_l^+$ .  $\theta_l^+$  is the angle between the lepton momentum  $\mathbf{p}_{l^+}$  in this frame and the boost direction  $\mathbf{z}_{W^+}$  from the  $t$  rest-frame to the  $W^+$  rest-frame.  $\phi_l^+$  is the azimuth angle of  $\mathbf{p}_{l^+}$  relative to the plane formed by  $\mathbf{z}_t$  and  $\mathbf{p}_{W^+}$  in the  $t$  rest-frame. The non-leptonic decays  $W^+ \rightarrow u\bar{d}$  or  $c\bar{s}$  can be specified by corresponding angles  $(\theta_l^+, \phi_l^+)$ , where the positive lepton label is replaced by the  $u$  or  $c$  quark. Since we have no ready means to distinguish a  $u$  from a  $\bar{d}$  jet, nor  $c$  from a  $\bar{s}$  jet, for pairs of jets, we have to add the rates for the angles  $\theta_q^+$  and  $(\pi - \theta_q^+)$  for  $q = u$  or  $c$ . Similarly, to specify  $W^- \rightarrow l^-\bar{\nu}_l$  in the  $W^-$  rest-frame, there are corresponding angles  $\theta_l^-$  and  $\phi_l^-$  whose definitions involve replacing  $t$  with  $\bar{t}$  and  $W^+$  with  $W^-$  in all of the above. Furthermore there are corresponding remarks that are appropriate for the decays  $W^- \rightarrow d\bar{u}$  or  $s\bar{c}$ .

Thus, each  $t\bar{t}$  final configuration requires the specification of eleven numbers

$$\left\{ \begin{array}{c} x \\ \theta \\ \bar{x} \end{array} \begin{array}{c} (\theta_W^+, \phi_W^+) \\ \\ (\theta_W^-, \phi_W^-) \end{array} \left\{ \begin{array}{c} (\theta_l^+, \phi_l^+) \text{ or } (\theta_u^+, \phi_u^+) \text{ or } (\theta_c^+, \phi_c^+) \\ \\ (\theta_l^-, \phi_l^-) \text{ or } (\theta_u^-, \phi_u^-) \text{ or } (\theta_c^-, \phi_c^-) \end{array} \right\} \right\} \quad (1.11)$$

if we sum over the spins of the initial  $q$  and  $\bar{q}$ , the spins of the  $t$  and  $\bar{t}$ , the spins of the final  $b$  and  $\bar{b}$ , and the spins of the final leptons  $l^+$  and  $l^-$  (or the spins of the quarks from non-leptonic decays). We note that, with the Standard Model, all the transitions occurring subsequent to the creation of the  $t\bar{t}$  system are completely prescribed in form and magnitude. These transitions have been fully described in an earlier publication (Dalitz & Goldstein 1992b). We emphasize that our calculations are carried out while retaining the spin and tensor polarizations of the  $W^\pm$  mesons, and repeat that we have always averaged over  $t$  and  $\bar{t}$  polarizations.

The final step involves the use of Bayes' Theorem, which gives the probability

distribution of mass  $m$ , given data on a set of events  $\{i\}$ . This theorem states that for an event  $i$

$$P(m|\text{data on event } i) = P(\text{observed event } i|m) \cdot \Phi(m), \quad (1.12)$$

where  $\Phi(m)$  represents the *a priori* probability that the top mass is  $m$ . For a set  $\{i\}$  of  $N$  events, this implies that

$$P(m|\text{data set } \{i\}) = \prod_{i=1}^N P(\text{event } i|m) \cdot \Phi(m). \quad (1.13)$$

In the following we use the notation  $P_i(m)$  for the distribution  $P(\text{event } i|m)$  for each individual event and we parametrise these distributions in a simple way, using two parameters,  $m_{pk}(i)$  and  $LIP(i)$ , defined below in Sec.2. We then determine how these and other possible parameters behave over a set of events.

Our purpose here has been to determine what behaviour we should expect for  $P(m|\text{data set } \{i\})$  when our analysis method is applied to a large ( $\approx 100$ ) batch of  $t\bar{t}$  production and decay events. This knowledge will allow us to discriminate between events which are due to production and decay of  $t\bar{t}$  systems from other events whose final states have the same leptons and quark jets, but which do not involve intermediate  $t$  and  $\bar{t}$  particles. Lacking guaranteed  $t\bar{t}$  production and decay events on which to test our method, we have had to generate a set of such events by computer simulation and to use them to test the method.

In Sec.2, we describe the procedure we followed to generate sufficiently large random samples of these events, using only the very simplest  $q\bar{q} \rightarrow t\bar{t}$  QCD graph, and the results found from our analysis of these events. The remarkable difference we find there between the outcome for dilepton events and the outcome for unilepton events (see Fig.3), appears to be in good qualitative accord with current experimental data (see Figs.6 and 9). In Sec.3, we illustrate our method by examining 3 dilepton events which have been reported in the literature (Abe *et al.* 1994b), commenting further on the additional 11 events which have become available since the 1997 Electron-Photon conference at Hamburg in July (Gironimi 1997). In Sec.4, we illustrate our method by examining seven unilepton events reported by CDF (Abe *et al.* 1994b), with conclusions in good general accord with those of CDF, except for one or two doubtful events, which might well not be due to  $t\bar{t}$  production and decay. In an Appendix we discuss an anomalous event in which a “secondary lepton” has low  $p_T$  for only one of the four jets, but has the wrong charge sign for this interpretation, and make out a quantitative case for regarding this lepton to be a “tertiary lepton”.

## 2. Monte Carlo Tests of our Analysis Procedures

With the likelihood methods we have proposed for the analysis of  $t\bar{t}$  production and decay events to determine the physical top mass  $m_t$ , it is essential for us to understand the quantitative significance of the values determined for the probability function  $P_i(m)$  from an experimental event labelled  $i$ . If a set of  $N$  events are all top-antitop events, the peak mass value  $m_{pk}$  for the product

$$P(m) = \prod_{i=1}^N P_i(m) \quad (2.1)$$

will be the Bayesian estimate for the top mass  $m_t$ . However, we require more than this. The peak probability values  $P_i(m_{pk}(i))$  for each event should have acceptable magnitudes and they must have a reasonable distribution over a set of  $N$  events. What these should be could best be established by making an analysis over some large batch of guaranteed events of this type. For this purpose, the only procedure available to us is to develop random sets of computer-generated events using a Monte Carlo (MC) simulation based on tree-level QCD Feynman graphs for top-antitop production, followed by their decay sequences (1.3) (1.4) and (1.5) to reach the final states “ $l^\pm$  4 jets” and “ $l^\pm l'^\mp$  2 jets”, in which the former has also one neutrino and the latter, where  $l'$  may or may not be the same as  $l$ , one neutrino and one antineutrino, unmeasured, and to carry out our analysis procedures on them, after making allowances for the proper development of the jets and the energy resolutions appropriate to the measurements of all the final particles. One may wonder whether such a simple ansatz as the single-gluon graph for  $\bar{q}q \rightarrow \text{gluon} \rightarrow \bar{t}t$  should be adequate for the description of top-antitop pair production in a proton-antiproton interaction at 1.8 TeV. Well, it is at least the simplest possible process existing within QCD, and a number of other proton-antiproton processes, not involving top quarks, have given data in quite a good agreement on the basis of cross sections calculated using QCD matrix-elements having the same degree of simplicity

(a) *The analysis procedure for unilepton events*

We began by generating 100,000 configurations for a mass  $m_0 = 170$  GeV assumed for the top quark, and divided them successively into five batches of 20,000. As remarked above, each configuration, say  $i$ , with  $i$  running from 1 to 100,000, requires the specification of the eleven possible variables (1.11), each of which varies over a finite range. If the lepton has charge  $+1$ , then  $(\theta_l^+, \phi_l^+)$  gives its direction of emission in the  $W^+$  rest frame, determined as specified in Sec.1. The corresponding  $W^-$  decays to  $(\bar{u}, d)$  or  $(\bar{c}, s)$ , with  $(\theta_u^-, \phi_u^-)$  or  $(\theta_c^-, \phi_c^-)$  now representing the direction of the  $\bar{u}$  or  $\bar{c}$  quark in the  $W^-$  rest frame. If the lepton has negative charge, then  $(\theta_l^-, \phi_l^-)$  specifies its direction of emission in the  $W^-$  rest frame, while  $(\theta_u^-, \phi_u^-)$  or  $(\theta_c^-, \phi_c^-)$  gives the direction of the  $u$  or  $c$  quark in the  $W^+$  rest frame. The finite 11-dimensional space of these variables was divided into a finite number of cells (Barger and Phillips 1987). Each event is assigned a weight  $w_i$ , which is equal to its fractional contribution to the theoretical total cross section. The aim is to make the cells about equal in net weight, summed over all the events in the cell, by changing the cell parameters as necessary. There is a convenient iterative procedure available, based on a program by Ohnemus (see Barger, Han, Ohnemus & Zeppenfeld 1990).

The first batch of 20,000 events led to a net weight in each cell, and a new set of partitions of the eleven variables were chosen, following Ohnemus, leading to a second set of cells, each with about the same weight. The next 20,000 events (batch 2) were then chosen and located in the new cells, leading to differing weights in these cells, so that a third set of partitions of the eleven variables had to be chosen, to even up the cell weights again. This procedure was iterated five times, for each new batch of randomly generated events. The distribution of the fifth batch of 20,000 events in the 11-dimensional space is then expected to be much closer to the physical reality corresponding to the simple tree-level model,

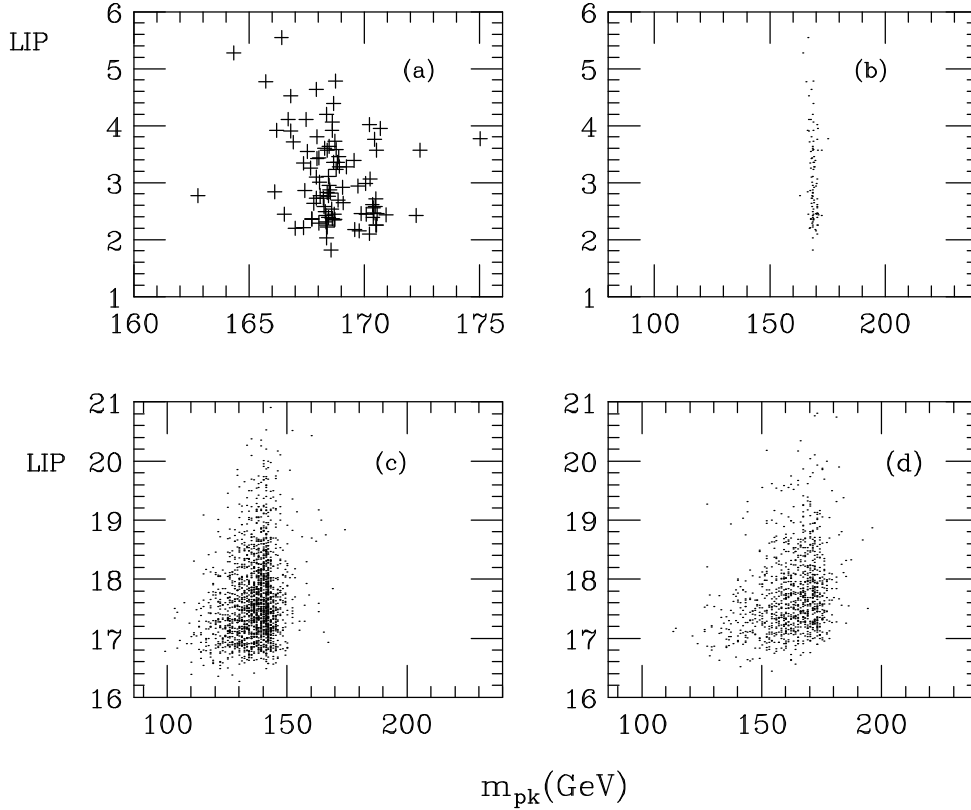


Figure 1. Scatter plots of  $LIP$  vs. peak mass  $m_{pk}$  analysed by our method for Monte Carlo-generated events, as follows: (a) for 95 unileptons, calculated for  $m_0 = 170$  GeV., (b) the same using a smaller abscissa, as for the following figures, (c) for 1899 dilepton events, calculated for  $m_0 = 140$  GeV., (d) for 1070 dilepton events, calculated for  $m_0 = 170$  GeV.

than that of the first 20,000 events. For each batch of configurations, and the events they give rise to, their number was reduced by requiring each event to satisfy experimental cuts that approximated those used by CDF for unilepton events. This reduces the size of each batch substantially. The cuts chosen required a minimum of 10 and 20 GeV/c transverse momentum for hadronic jets and leptons, respectively, a minimum pseudorapidity separation from one outgoing particle to another of 2.5 units, and a minimum separation between jets of 0.7 units in the pseudorapidity-azimuthal angle plane. Now the improvement achieved in each iteration can be tested, for example by comparing the total cross section calculated after each iteration with the directly calculated total cross section for this simple model.

We then chose arbitrarily all those events from batch 5 which survived the cuts applied experimentally to unilepton events and which bore a number between 80,000 and 83,000. These events were 1292 in number, each with its own  $w_i$ . We then made use of these weights to obtain a smaller set of unweighted events to form a representative subsample. The largest unilepton subsample we can analyze is about 100, rather than 1000, since our analysis procedure is quite complicated and takes more computer time than does the analysis of dilepton events to be discussed in subsection 2(b). We assigned a random number  $v_i$  between 0 and 1

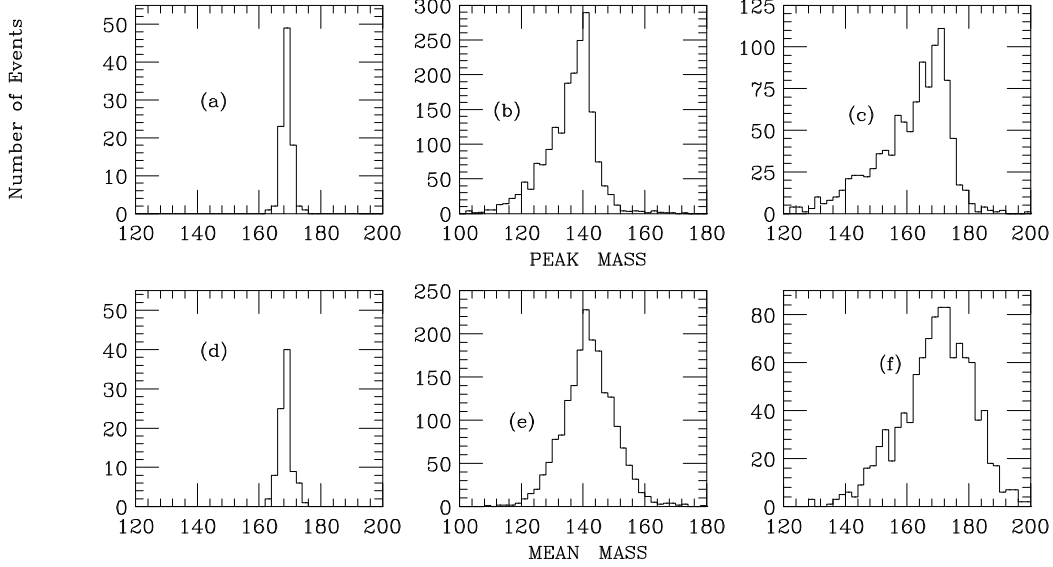


Figure 2. Projection of the scatter plots of Fig.1 onto the  $m_{pk}$  axis - (a) for 1(b), (b) for 1(c), the case  $m_0 = 140$  GeV, and (c) for 1(d), the case for  $m_0 = 170$  GeV. The analogous projections from the  $(\bar{m}(i), LIP(i))$  scatter plots, not shown here, using mean masses  $\bar{m}(i)$ : (d), (e) and (f).

to each of the chosen events (here 1292) and rejected those for which  $v_i$  exceeds  $w_i$  (Barger & Phillips 1987). This left a subsample of 95 unilepton events which was a manageable batch. Our purpose then was to compare the observed features of the candidate top-antitop events with the features predicted for these events by the QCD model.

Since these were MC events, we know which quarks are which. In analyzing each unilepton event, typical energy measurement errors are assumed for the lepton and the jets but angles are accepted “as is”, since their measurement is much more accurate than those for energies. The jet energies are assumed to have a Gaussian distribution in magnitude, which is represented by taking 10 points about the central value, weighted to give a discrete approximation to a Gaussian with the known standard deviation  $\sigma(E) = 3.4 + 0.1E$  GeV. We then used our analysis method (Dalitz & Goldstein 1994, 1992a,b and Goldstein, Sliwa & Dalitz 1993) to deduce the probability distribution  $P_i(m)$  for each unilepton event, where  $m$  denotes the mass variable. The parameters  $m_{pk}(i)$  for the peak of  $P_i(m)$  and  $IP(i)$ , the integrated probability given by

$$IP(i) \equiv \int dm P_i(m), \quad (2.2)$$

are convenient for specifying concisely the most characteristic features of the probability distribution  $P_i(m)$  deduced for an event  $i$ . In practice we have found it more convenient to use  $LIP$ ,  $\log_{10}$  of the integrated probability, defined in

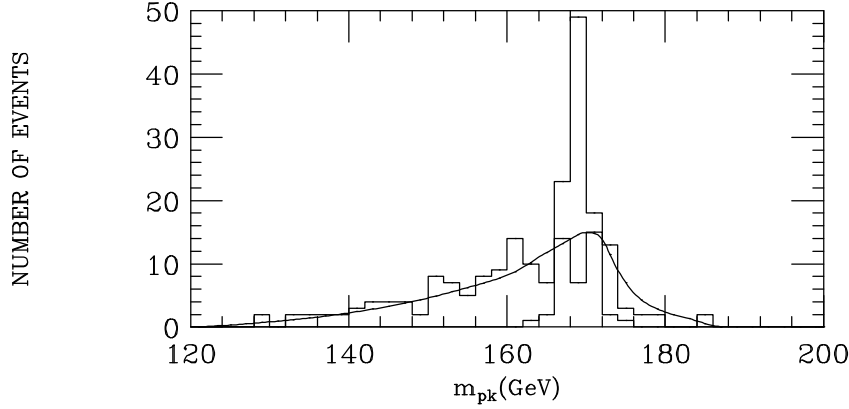


Figure 3. The distributions of  $m_{pk}$  for 153 Monte Carlo dilepton events (broad histogram), 95 Monte Carlo unilepton events (central histogram), and for 1070 Monte Carlo dilepton events scaled to 153 events and smoothed (solid curve).

eq.(2.2) above, as our second parameter. We note again the notation  $m_0$  for the input top quark mass for the Monte Carlo generation of our sample of events for testing our procedure. Other parameters of relevance are the mean mass  $\bar{m}(i)$  for the  $i$ -th event

$$\bar{m}(i) = \frac{\int m P_i(m) dm}{\int P_i(m) dm}, \quad (2.3)$$

while the mean value of all the  $\bar{m}(i)$  in a batch of  $N$  events is

$$\langle \bar{m} \rangle = \left( \sum_{i=1}^N \bar{m}(i) \right) / N \quad (2.4)$$

For our 95 unilepton Monte Carlo events, a scatter plot showing the distribution of the two parameters  $m_{pk}(i)$  and  $LIP(i)$ , is displayed in Fig.1(a) and again in 1(b). This shows that the MC event-points are very localized in mass, but widely spread in  $LIP$ . This is clear in Fig. 2(a), which shows the projection of event-points on the  $m_{pk}$  axis (such a distribution of mass values will be called  $\mathcal{P}(m_{pk})$  in the following), and is emphasized further in Fig. 3, where the central histogram shows that there is a sharp peak in  $\mathcal{P}(m_{pk})$  at approximately 168.4 GeV, only 1.6 GeV below the input mass  $m_0 = 170$  GeV, the mass value for which these MC events were computed. The  $LIP$  distribution, obtained by projecting the scatter plot on the  $LIP$  axis, is shown in fig. 4(a).

The integrated probability values  $IP(i)$  given here may appear unreasonably small, at first sight, but these are the values which result from the analysis of our Monte Carlo generated events. To the extent that the latter are representative of real top-antitop events, these magnitudes will be typical of the  $\log(IP)$  values deduced from real events, and this will be illustrated by the application of our analysis method to the real events available, in Sections 3 and 4. This is the underlying logic of our method. If we had a large sample of top-antitop candidates, which happened to yield  $m_{pk}$  values in the mass region of interest for top, say  $\sim 170$  GeV, the evaluation of the  $LIP = -\log_{10}(IP)$  for them would constitute a test of their interpretation as top-antitop events. If these  $LIP$  values did not



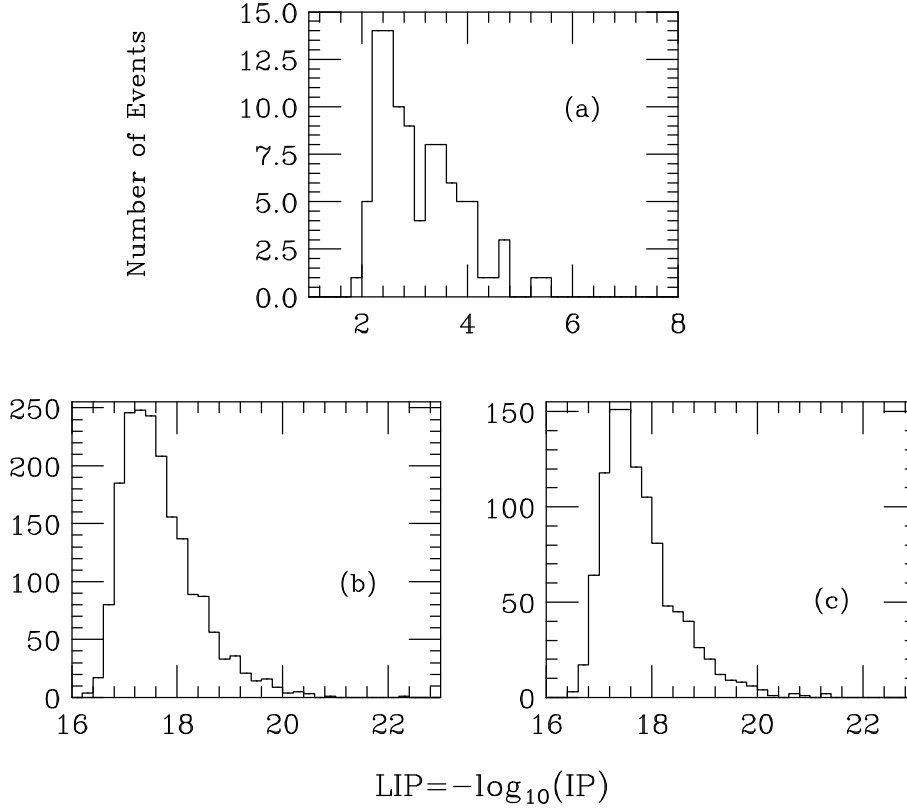


Figure 4. The projection of the scatter plots onto the  $LIP$  axis (a) from 1(a) for 95 unilepton events with  $m_0 = 170$  GeV, (b) from 1(c), for 1899 dilepton events with  $m_0 = 140$  GeV, (c) from 1(d), for 1070 dilepton events with  $m_0 = 170$  GeV.

follow the  $LIP$  distribution shown here in fig. 4(a), these candidate events could not be accepted as top-antitop production and decay events.

#### (b) The analysis procedure for dilepton events

For dilepton events, we used the same randomly chosen sets of eleven numbers (1.11) to define 100,000 configurations for the dilepton events. Both  $(\theta_l^+, \phi_l^+)$  and  $(\theta_l^-, \phi_l^-)$  are for leptons, the former for the  $l^+$  from the  $W^+$  and the latter for the  $l^-$  from  $W^-$  decay. This change from the case of unilepton events affects both the kinematics of the event and the cross section calculated for it using our simple QCD model. Some of the cuts to be applied also change when a  $q\bar{q}$  pair is replaced by a lepton pair ( $l\nu_l$ ), a further change to the input cross sections.

As in the unilepton case, these 100,000 event configurations were divided into 5 batches of 20,000 events. The first batch led to a net weight, different from that for the unilepton case, in each initial cell. A second set of partitions of the variables (1.11) were chosen, leading to a second set of cells which are different from the second set for the unilepton case and which also lead to differing weights in these cells. A third set of partitions of the variables (1.11) has to be chosen and so on, to the fifth batch. We then assigned a random number  $v_i$ , between 0 and 1, to each of the 12,503 events surviving the cuts in this batch, and rejected those for which  $v_i$  exceeds the weight  $w_i$  (Barger & Phillips 1997). This left us with a random

Table 1. *Iterations of Monte Carlo simulation for dilepton events*

(Averaging over the batches 6 to 10 gives the more definite value 4.718 pb for  $10^2 \cdot \sigma_{net}$ , with  $10^2 \cdot \text{fluctuation}$  reduced to 0.018.)

batch no.	1	2	3	4	5
$100 \cdot \sigma_{net}(pb)$	4.595	4.766	4.767	4.710	4.733
100-fluctuation	0.133	0.059	0.045	0.040	0.039
batch no.	6	7	8	9	10
$100 \cdot \sigma_{net}(pb)$	4.716	4.683	4.760	4.714	4.716
100-fluctuation	0.039	0.039	0.039	0.040	0.040

subsample of 1070 dilepton events for analysis. In this analysis we did not include simulated measurement errors, both because the samples of dilepton events need to be larger, for reasons to be seen below, and because of time constraints on the computations. The scatter plot for the  $(m_{pk}, LIP)$  values obtained for those 1070 events is shown on Fig. 1(d). We note that the mass distribution obtained from the dilepton events shown in Fig. 2(c) is very much broader than that shown in Fig. 2(a) for unilepton events. This is emphasized again in Fig. 3, where we have plotted the distributions of peak masses,  $\mathcal{P}(m_{pk})$ , for both the 95 unilepton events and the dilepton plot of 1070 events but scaled to 153 events. The great breadth of  $\mathcal{P}(m_{pk})$  for dileptons - the FWHM estimated from Fig. 2(c) is about 15 GeV, compared with about 4 GeV for  $\mathcal{P}(m_{pk})$  for unileptons - means that many more dilepton events must be available for measurement, by about one order of magnitude, to gain the same statistical accuracy for the top mass as with unilepton events. Balanced against this is the fact that dilepton candidate events suffer less from background than is the case for unilepton candidate events.

The dilepton mass distribution  $\mathcal{P}(m_{pk})$  also shows very considerable asymmetry, in general. For  $m_0 = 170$  GeV, the mean peak mass  $\langle m_{pk} \rangle$  for 1070 events is 162.0 GeV and the median of the peak mass distribution is 165.0 GeV, both well below the peak mass deduced to be approximately 171 GeV. Indeed, we find that 74% of the dilepton events for  $m_0 = 170$  GeV give peak mass values below  $m_0$ . With small samples of dilepton events, it is therefore natural to find lower top mass values than those from comparable samples of unilepton events. We had noted this disconcerting tendency in our earlier work on the analysis of dilepton candidate events (Dalitz & Goldstein 1995).

We have carried out calculations similar to the above, for 100,000 dilepton events with  $m_0 = 140$  GeV. The resulting scatter plot is given in Fig. 1(c); the number of events plotted is 1899, and the mass distribution  $\mathcal{P}(m_{pk})$  appears much sharper than for  $m_0 = 170$  GeV. For both  $m_0 = 140$  and 170 GeV, the peak obtained for  $\mathcal{P}(m_{pk})$  is in the bin  $(m_0, m_0 + 2)$  but its distribution lies mostly below  $m_0$ , being markedly asymmetric. The mean mass  $\langle m_{pk} \rangle$  is 136.1 GeV and the median is 138.0 GeV.

To investigate the convergence of the iterative procedure used, we went on to

generate another 100,000 dilepton configurations for  $m_0 = 170$  GeV, dividing them into five batches of 20,000 and starting from the cells obtained from the fifth batch of the first 100,000 configurations. The calculations of the total cross section are extended in Table 1 up to the tenth iteration. We note that the fluctuations in the test function (here the total cross section) from batch to batch are considerable, but that a value accurate to 2% is achieved after the first five batches; taken together the last 5 batches reduces the accuracy to 1%. With cuts similar to these, the total cross section for dileptons has been calculated as a function of the top mass by several groups (Berends *et al.* 1991, Han & Parke 1995), using the same QCD tree-level model; reading from their graph, their results are about 0.05 pb. for  $m_0 = 170$  GeV and c.m. energy 1.8 TeV. Another test function could be provided by  $\mathcal{P}(m_{pk})$ , the probability function for the top mass. With this we found that there was a significant change in  $\mathcal{P}(m_{pk})$  after the first iteration; but that thereafter,  $\mathcal{P}(m_{pk})$  varied moderately from batch to batch but without any clear convergence to a limit.

(c) *Peak Masses or Mean Masses?*

One obvious difficulty about using peak mass values  $m_{pk}(i)$  is that the  $P_i(m)$  distributions obtained tend to have spiky and/or multiple peaks, as is apparent from Fig. 8. This has the consequence that the  $m_{pk}(i)$  can be strongly affected by statistical fluctuations, a rather unsatisfactory situation. The use of the mean mass  $\bar{m}(i)$  does not suffer from this defect, but, of course, it represents a departure from the use of the Bayes Theorem. However, it is useful to trace here the effects its use would have with our Monte Carlo generated events. The event-points scatter more widely when we use the scatter plot for  $(\bar{m}(i), LIP(i))$  rather than  $(m_{pk}(i), LIP(i))$ , but the main contrast is in the distribution of  $\bar{m}(i)$ ,  $\mathcal{P}(\bar{m})$ . These features can be seen clearly in the  $\bar{m}_i$  mass distribution shown in Fig. 2(d,e,f). There is only a slight broadening to be seen for the unilepton case, but the dilepton  $\mathcal{P}(\bar{m})$  for  $m_0 = 170$  GeV is much more symmetric than the  $\mathcal{P}(m_{pk})$  distribution; its peak value is  $(\bar{m})_{pk} = 172$  GeV, its FWHM being about 23 GeV, and its mean value is  $\langle \bar{m} \rangle = 169.5$  GeV. The latter would appear to be quite a reliable indicator for the top quark mass. A batch of about 25 events, at least in ideal circumstances, should be sufficient to determine  $\langle \bar{m} \rangle$  to an accuracy of  $\pm 2.5$  GeV. However, to determine  $m_t$  from this quantity requires a knowledge of  $\Delta(m_t) = \langle \bar{m}(m_t) - m_t \rangle$  as a function of  $m_t$ , which can be taken from the analysis of Monte Carlo events discussed above; we have determined  $\Delta(m_t)$  for the values  $m_t = 170$  GeV and (see below) 140 GeV. This requires some dependence on theoretical calculations, but at least the dilepton events do have a low background.

The  $LIP$  distribution for dileptons, shown in fig. 4(c), is not unlike that for unileptons in shape. The difference in its normalization between these two cases is unimportant; what matters is that the same normalization should be adopted for the analysis of real events as for the normalization of our Monte Carlo events.

As shown in Figs. 1(c), 2(b,e) and 4(b), we have also carried out analyses for a comparable body of Monte Carlo unilepton and dilepton top-antitop events for  $m_0 = 140$  GeV. The  $m_{pk}(i)$  distribution is asymmetric, but not as much as for  $m_0 = 170$  GeV; the  $\bar{m}(i)$  distribution in Fig.2(e) is symmetric, with peak in the bin (140, 142) and with mean value at 142.0 GeV and median value 141.7 GeV.

The scatter plots display a single mass value for each event, either the peak or the mean value, as well as the *LIP*. However, the full distribution  $P_i(m)$  for a single event  $i$  contains more information than these two numbers. In principle, we should consider the product of all  $P_i(m)$  for a fixed  $m$ , and use this joint probability in making deductions from the data. We illustrate this procedure in Sec.4.

What we have gained from this analysis of Monte Carlo  $t\bar{t}$  events is some feeling for what variations in *LIP* and  $m$  may arise from purely statistical origin. For either dilepton or unilepton events, the *LIP* can vary from its mean value within about  $\pm 1$ . For the unilepton events, the peak mass determined will lie very close to the top mass, within several GeV below, whereas the mass value determined from dilepton events has a larger range of variability.

### 3. Data and Analyses for Dileptonic Events

In this Section, we shall discuss what light the Monte Carlo model calculations above may throw on the interpretation of the dileptonic events believed to represent top-antitop production and decay in proton-antiproton collisions with energy 1.8 TeV. The final states are

$$(i) \quad b\bar{b}l_1^+\nu_1l_2^-\bar{\nu}_2 \quad \text{or} \quad (ii) \quad b\bar{b}l_2^+\nu_2l_1^-\bar{\nu}_1. \quad (3.1)$$

where the leptons  $(l_1, l_2)$  may be two different species,  $(\mu^\pm, e^\mp)$ , or the same species, thus  $(e^+, e^-)$  or  $(\mu^+, \mu^-)$ . For the latter it is necessary to avoid  $e^+e^-$  and  $\mu^+\mu^-$  pairs arising from the production and decay of  $J/\psi$  mesons, by the use of cuts to exclude them.

These events (3.1) have two hadronic jets, one generated by the  $b$  quark and the other by the  $\bar{b}$  quark, and it is of importance to identify which jet stems from which quark. There are a number of ways to achieve this. The most direct uses the fact that the  $b$  quark has quite a long lifetime  $\tau_b \sim 1.6 \times 10^{-12}$  sec. At the high energies in 1.8 TeV collisions, the flight path of the  $b$ -system will be of order  $5(E_b/m_b) \times 10^{-2}$  cm, a macroscopic distance which can frequently be observed with the use of a specially designed Silicon Vertex Detector. CDF has had such a detector in place during its runs over the last two years, referred to as an SVX, and its effectiveness has been great, as is indicated by CDF's report that it has efficiency of 40% for the identification of  $b$  and  $\bar{b}$  decay vertices in the events (3.1). This is termed an "SVX-tag". The other instrumental means for determining the  $(b, \bar{b})$  assignments to the two jets is the observation of the charge sign for a secondary lepton arising from the subsequent decay  $b \rightarrow l^+$  or  $\bar{b} \rightarrow l^-$ . Since the energy released in these decays is relatively small, the path of the secondary lepton is generally close in direction to that of the parent quark jet, while its charge identifies its quark origin. This is known as a Secondary Lepton Tag, SLT for short. It is a powerfully informative tag but its efficiency is lower, being about 20%, as CDF reports.

Other means exist for deciding which is the  $b$ -quark, from internal evidence about the event, in its analysis. For example, our analysis procedure involves taking the lepton  $l_1^+$  together with a jet, say  $j_1$ , and determining the spatial circle  $E_{1+}$  on which the total momentum  $(\mathbf{P}_{j_1} + \mathbf{I}_1^+)$  must lie if its parent  $t$  quark mass is  $m_1$ , and then taking the lepton  $l_2^-$  with the other jet and determining

the spatial circle  $E_{2-}$  on which the total momentum  $\mathbf{P}_{j2} + \mathbf{l}_2^-$  must lie if their parent  $t$ -quark mass is  $m_2$ . If this event really is  $(t + \bar{t})$  decay, then  $m_1 = m_2 = m$ . Further, the momentum  $(\mathbf{t} + \bar{\mathbf{t}})_T$  transverse to the initial proton-antiproton axis is necessarily very limited in magnitude and might even be constrained to be zero, in first approximation, in which case the possible transverse momenta  $(\mathbf{P}_{j1} + \mathbf{l}_1^+)_T$  and  $(\mathbf{P}_{j2} + \mathbf{l}_2^-)_T$  are given by the intersections of the two ellipses obtained by projecting the spatial circles  $E_{1+}(m)$  and  $E_{2-}(m)$  onto the transverse plane. These two projected ellipses may have 4, 2 or 0 intersections, depending *inter alia* on the value of  $m$ . If they have no intersection for any  $m$ , this just means that this pairing of the leptons with the jets is not consistent with a  $t\text{-}\bar{t}$  origin. However, it is also possible to associate the pairs  $(\mathbf{P}_{j2} + \mathbf{l}_1^+)$  and  $(\mathbf{P}_{j1} + \mathbf{l}_2^-)$  instead, to repeat these steps with them, and to find the resulting ellipses do have sensible intersections. If this is the case, we can conclude that  $j_2$  is the  $b$ -jet and that  $j_1$  is the  $\bar{b}$ -jet. This is the case for the event 19250, for example.

Since there are generally ranges of  $m$  for which the projected ellipses have two intersections (and sometimes even ranges where there are four intersections, although this is rare), we can take this line of argument a step further. For each corresponding solution as a function of mass  $m$ , there will be a value for  $LIP$ . If there is a solution for which  $|LIP|$  is much lower than all other solutions, it is natural, following the Bayesian principle, to confine attention to this solution. This choice represents a definite assignment of the jets ( $j_1, j_2$ ) to the quarks ( $b, \bar{b}$ ).

We give on Table 2 the lepton and jet energies and momenta for the three early CDF events, for illustration. The event 47122 is a normal event. The jet 1 is associated with  $e^+$ , so that it is the  $b$ -jet; the jet 2 is associated with  $\mu^-$ , and it is the  $\bar{b}$ -jet. The jet 3 has an exceedingly large longitudinal momentum with a modest transverse component  $|P_{3T}| = 18$  GeV, making an angle of 4 degrees with the initial  $p\bar{p}$  axis, and belongs to the remnants of the antiproton after the collision. The event 19250 has a secondary  $\mu^+$  lepton of energy 30 GeV which is clearly associated with the  $\bar{b}$ -jet of energy 71 GeV, its transverse momentum to the  $\bar{b}$ -jet being only 4 GeV. The third event, 41540, also includes a third jet of energy 247 GeV which makes only a 6 degree angle with the initial  $p\bar{p}$  direction and clearly belongs to the antiproton remnants after the collision. Its second  $\mu^+$  meson is anomalous, since it is not associated with jet-2 and we shall comment further on this event in the Appendix.

We have analysed these three events by the same procedure as outlined in the Monte Carlo section (Dalitz & Goldstein 1992a,b,1994). We assigned uncertainties to the jet transverse energies by the same algorithm as above. The resulting probability distributions are shown in Fig. 5. In each case, the assignment of jets to the  $b$  and  $\bar{b}$  quarks is uniquely determined by this analysis. The probability distributions  $P(m)$  from these CDF events, shown in Fig.5, peak at 158 GeV, with  $LIP = 20.0$  for 41540, at 168 GeV, with  $LIP = 17.4$  for 47122 and at the low mass of 121 GeV, with  $LIP = 16.8$ , for 19250. The joint probability for these three events is the product of their separate probabilities and  $\log_{10}(\text{joint probability})$  for them is plotted vs.  $m$  as Fig.5(d), peaking at about 158 GeV. These three early events illuminated well the tendency for small sets of dilepton events to indicate lower  $m_t$  values than the unilepton events, using our Bayesian method.

At the 1997 Electron-Photon Conference at Hamburg, CDF reported on 9

Table 2. *Dilepton event data reported by CDF (Abe, et al. 1990, 1994b; Sliwa 1991)*

(Comments on the right are from CDF. Elsewhere in the text we shall identify each event by its run number only; events are so rare that, to date, identification by run number has been unique.)

	$p_x$	$p_y$	$p_z$	$E(\text{GeV})$	
Run 19250 Event 20425					
$e^+$	-21.2	23.6	-28.6	42.7	
$\mu^-$	-0.6	-43.7	-38.6	58.3	
jet 1	18.7	-6.3	25.3	33.3	
jet 2	0.7	8.9	-70.1	70.7	
$\mu^+$	-1.0	7.9	-28.7	29.8	
Run 41540 Event 127085					
$e^-$	18.7	11.7	20.7	30.2	
$\mu^+$	46.1	11.5	8.1	48.2	
$\mu^+$	8.7	-1.2	1.6	8.9	soft $\mu^+$
jet 1	129.7	-18.2	14.4	131.8	with $\mu^+$
jet 2	-50.0	-35.0	-34.6	70.1	with $e^-$
jet 3	-9.7	24.1	-245.2	246.6	backward anti-proton jet
Run 47122 Event 38382					
$e^+$	45.9	21.4	54.1	74.1	
$\mu^-$	37.2	2.6	-30.2	48.0	
jet 1	-67.0	-52.3	58.2	103.0	with $e^+$
jet 2	25.0	-7.2	46.2	53.1	with $\mu^-$
jet 3	17.3	-5.0	-246.1	246.8	backward anti-proton jet

dilepton events which included the two events previously reported—7  $e^\pm\mu^\mp$ , 1  $e^+e^-$  and 1  $\mu^+\mu^-$ —and a preliminary report on their details is given in a Ph.D dissertation (Kruse 1996). D0 reported on 5 dilepton events—3  $e^\pm\mu^\mp$ , 1  $e^+e^-$  and 1  $\mu^+\mu^-$ —and a preliminary report on their details is given in a Ph.D. dissertation (Varnes 1996), available on the Internet. We have made our own analysis of these events, with results quite similar to those reported recently, as just mentioned. We give a plot of the  $m_{pk}$  values for 15 dilepton events in Fig. 6. They are distributed very broadly, which we had anticipated following our analysis of MC-generated QCD events in Sec. 2 above. This supports our conclusion that small samples of dilepton events are bound to give mass values substantially below the top quark mass. It is noticeable that the mass values reported by D0 lie systematically above those reported by CDF; of 5 D0 events, 3 lie above all of the CDF values, and one of these is very high, isolated at 200 GeV. The median mass for this plot lies in the 155-160 GeV bin and this does not change if we cut off its extreme values, two in the 120-125 bin and three at masses 185, 185 and 200 GeV. We note only that the mass plot is in good qualitative accord with expectation. Unfortunately, we do not yet have Monte-Carlo calculations for  $m_0 > 170$  GeV but expect that the

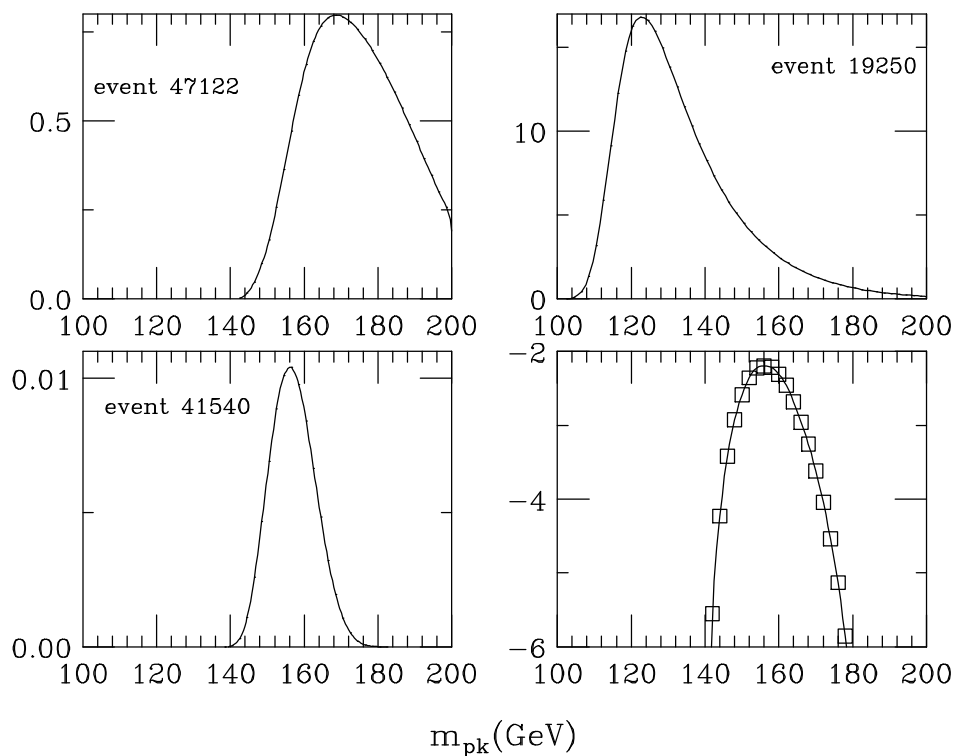


Figure 5.  $P_i(m)$  for three CDF dilepton events (note that we use CDF's run number to label the event). The lower right figure is the logarithm of the product of the three probabilities.

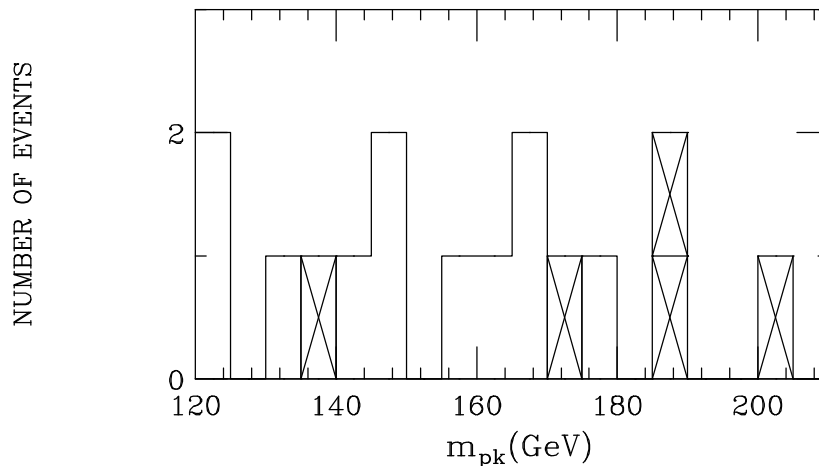


Figure 6. The distribution of  $m_{pk}$  values determined from the 16 dilepton events available empirically. The D0 events are marked with an X.

curve for  $m_0 = 180$  GeV will be close to that obtained by expanding elastically the plots for  $m_0 = 170$  GeV in the variable  $m$ .

Finally, we turn to the projection of the scatter plot onto the  $LIP$  axis, shown for the CDF and D0 data on Fig. 7. This is to be compared with the distributions in Fig. 4 which we have calculated for the values  $m_0 = 140$  and  $170$  GeV. For

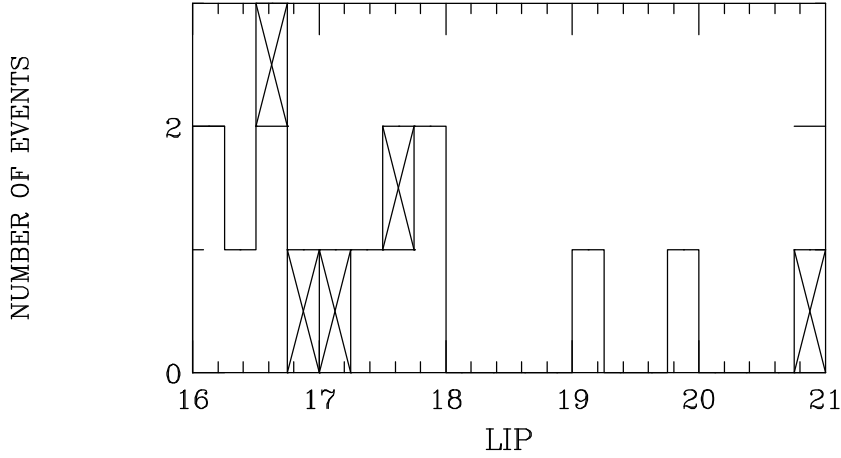


Figure 7. The distribution of  $LIP$  values determined from the 16 dilepton events available empirically. The D0 events are marked with an X.

both of these, the peak in  $LIP$  was found to be about  $LIP = 17.2$ , the rapid rise from below being at about  $LIP = 16.8$ . The empirical values for  $LIP$  are of the right order-of-magnitude but appear to be smaller than the calculated values by about 0.8.

#### 4. Data and Analyses for Unilepton Events

In this Section, we discuss the available data on the final states

$$(a) \quad b(l^+\nu_l)\bar{b}(\bar{q}q), \quad (b) \quad b(\bar{q}q)\bar{b}(l^-\bar{\nu}_l) \quad (4.1)$$

which result when one  $W$ -decay is leptonic, for  $l = e$  or  $\mu$ , and the other  $W$ -decay is to two hadron jets, in the light of our model calculations described in Sec. 2 above. The states (4.1) have the advantage that there is only one neutrino, but they also have the disadvantage that there are four jets to be identified. It is clear that  $b$ -tagging is the vital key to their unique, or most probable identification.

The data on unlepton events reported at the lepton-photon conference at Hamburg (Geromini 1997) are now quite large in number. The CDF collaboration reported 22  $b$ - and/or  $\bar{b}$ -tagged events, made up of 12 events with a single SVX-tag, 8 with a single SLT-tag and 2 with a double tag. This includes the 7 tagged events reported earlier (Abe *et al.* 1994b), when their SVX detector was already in use. With allowance for background, CDF have used their events to give an estimate of the top mass, namely  $m_t = 176.8(4.4)$  GeV. The D0 collaboration reported on 11 events, 5 having a primary electron and 6 having a primary muon, on the basis of which they made the estimate  $m_t = 173.3^{+5.6}_{-6.2}$  GeV. Neither CDF nor DO reported on individual unlepton events beyond CDF's 7  $b$ -tagged events just mentioned, so we are necessarily limited to the discussion of the latter.

To illustrate the above remarks about unlepton event analyses, we apply our procedure to the available data, the 7 such events published in full by CDF (Abe, *et al.* 1994). In Table 3, we lay out these data, in a form convenient for use. All 7 events are  $b$ -tagged, three are SLT-tagged, three are SVX-tagged, and one is both SLT- and SVX-tagged.

The jet calorimeter energies are the "corrected values" quoted by CDF (Abe *et*



Table 3. *Single lepton data (Abe et al. 1994b)*

(In each event (identified by run number) one jet was tagged as a  $b$ -jet via the Silicon Vertex Detector (SVX) or the emission of a Soft Lepton (SLT). The  $j1, \dots$  labels correspond to CDF's jet numbers.)

event		$p_x$	$p_y$	$p_z$	$E(\text{GeV})$		
40758	$e^+$	-94.313	-50.113	48.523	117.306	SVX	
	jet j1	86.267	26.685	-21.881	92.913		
	j2	-26.220	74.310	23.996	82.373		
	j3	46.052	47.417	43.659	79.217		
	j4	30.613	-22.003	76.790	85.545		
43096	$e^-$	21.753	21.093	-27.316	40.795	SVX	
	j1	78.068	100.425	2.544	127.225		
	j2	-70.137	29.785	137.091	156.845		
	j3	10.642	-66.960	81.787	106.235		
	j4	-34.707	-14.202	138.856	143.831		
43351	$\mu^-$	24.577	-1.062	-1.723	24.660	SLT	
	j1	109.365	-75.333	195.687	236.494		
	j2	-85.879	6.159	-15.582	87.499		
	j3	24.815	-21.905	7.680	33.979		
	j4	-3.595	36.122	14.128	38.953		
	$\mu^-$	-0.605	2.032	1.057	2.369		$p_{t\perp} = 0.46$
45610	$\mu^+$	52.325	11.153	-9.682	54.369	SVX	
	j1	11.612	76.423	-58.639	97.025		
	j2	-13.843	-71.064	-74.320	103.755		
	j3	3.167	-36.061	-77.935	85.932		
	j4	-19.286	-9.042	1.492	21.352		
45705	$e^-$	12.221	54.445	42.329	70.038	SLT	
	j1	-74.864	-49.953	81.137	121.174		
	j2	-51.229	4.189	-11.399	52.649		
	j3	15.072	-54.971	41.817	70.694		
	j4	31.974	-9.305	113.471	118.256		
	$e^+$	1.523	-10.995	8.984	14.280		$p_{t\perp} = 1.62$
45879	$\mu^+$	52.586	4.746	-11.170	53.969	SVX & SLT	
	j1	-75.575	27.724	-197.545	213.317		
	j2	45.871	-84.446	-10.592	96.682		
	j3	33.259	25.812	5.488	42.456		
	j4	-36.642	-4.359	-16.765	40.530		
	$\mu^-$	6.680	-11.732	-1.488	13.582		$p_{t\perp} = 0.27$
45880	$e^-$	-5.942	-25.106	4.146	26.131	SLT	
	j1	98.037	-7.188	-19.791	100.273		
	j2	-26.071	-55.037	80.329	100.804		
	j3	18.082	39.344	16.853	46.464		
	j4	-22.051	-13.776	-16.246	30.658		
	$e^-$	0.838	2.440	1.088	2.800		$p_{t\perp} = 0.27$

*al.* 1994b) in their Appendix A, following the calculated scatter plots given in their Fig. 57; they are the CDF estimates for the original parton energies, with well defined statistical uncertainties. The c.m. energy for the two jets hypothesized to result from  $W$  decay is generally rather far from the well-known value (Particle Data Group 1996)  $M_W = 80.2(2)$  GeV, and this presents a problem. CDF uses a kinematic fitting procedure, established long ago (Dahl *et al.* 1968) in bubble chamber work, to manipulate the already corrected transverse energies in order to reproduce the  $W$  mass value at the expense of a higher  $\chi^2$ . We do not use the resulting “best fit values” given by CDF, since we follow a different scheme of analysis (Dalitz & Goldstein 1994).

Our analysis of these  $l^\pm 4j$  events (4.1) employs a simple extension (Goldstein *et al.* 1993) of the method used for dilepton events. We sketch it briefly here, for the case of a positively charged lepton  $l^+$ ; the case for  $l^-$  follows when every particle is replaced by its antiparticle and vice versa. One jet chosen tentatively to be the  $b_l$  jet associated (using the CDF notation (Abe *et al.* 1994b)) with  $l^+$  and a kinematic paraboloid is formed, as before, leading to an ellipse in momentum space which includes all momenta  $\mathbf{t}$  consistent with  $\mathbf{b}_l$  and  $l^+$ , for an assumed mass  $m_t$ . The other three jets are assumed to arise from  $\bar{t}$  decay where the resulting  $W^-$  boson decays hadronically, thus:

$$\bar{t} \rightarrow \bar{b} + W^-, \quad \text{followed by} \quad W^- \rightarrow \bar{q}_1 + q_2. \quad (4.2)$$

The quark assumed to be  $\bar{b}$  will be denoted by  $b_j$ . The experimental error distributions for these quark energies have been discussed in much detail by CDF (Abe *et al.* 1994b) and we adopt the same algorithm that interpolates their  $\sigma_E$  values as stated in Sec. 2. A grid of momentum values  $(\bar{\mathbf{b}}, \bar{\mathbf{q}}_1, \mathbf{q}_2)$  is laid out and weighted by their probability values at each point, together with a probability weighting  $F_W(\bar{q}_1, q_2)$  of Breit-Wigner form to emphasize those grid points at which  $(\bar{q}_1, q_2)$  is consistent with the  $W$ -boson mass. At each grid point, there is a definite momentum  $(\bar{\mathbf{t}} = \bar{\mathbf{b}} + \bar{\mathbf{q}}_1 + \mathbf{q}_2)$  and deduced mass  $m$ , and this point is then paired with the points on the  $t$ -ellipse for  $m$ , which also have their weighting factors due to measurement errors. This product of probabilities is finally weighted by a Gaussian factor  $G[|(\mathbf{t} + \bar{\mathbf{t}})_{\mathbf{T}}|/\rho]$  to represent the effect of limited transverse momentum due to initial state gluon emission, the value  $0.1m$  being adopted for the parameter  $\rho$ . Contributions to the net probability for the top quark mass to lie within  $(m, m + \Delta m)$  come from all grid points which lie within the band  $\Delta m$ , and are summed to give the net probability  $P_i(m)$  indicated by this event.

For a real event having a primary lepton  $l^+$ , the probability must be computed separately for each possible assignment  $(b_l; \bar{q}(1), q(2), b_j)$  to the four outgoing quark jets labelled arbitrarily as j1, j2, j3 and j4. Here  $b_l$  denotes the jet arising from the decay  $t \rightarrow bW^+ \rightarrow b_l(l^+\nu_l)$ , while  $\bar{b}_j$  denotes the jet arising from the decay  $\bar{t} \rightarrow \bar{b}W^- \rightarrow \bar{b}_j(\bar{q}(1)q(2))$  where the  $q(i)$  are the light quark jets ( $\bar{u}(1)d(2)$  and  $(\bar{c}(1)s(2))$ ). At the Tevatron, the primary lepton will generally have high energy, typically of order 40 GeV, and a large  $p_T$  with respect to each of the four jets. For a real event with a primary lepton  $l^-$ , the assignments are  $(\bar{b}_l; q(1), \bar{q}(2), b_j)$ , the quarks for the  $l^+$  case being replaced by antiquarks and vice versa. If the primary lepton charge is known, as is usual, and none of the jets are b-tagged, there will be 24 permutations to consider for the identities of the four jets, with 24 different probabilities, in general. Most of these 24 possibilities will not provide a fit to the

event, or at most a very poor fit; the constraint that the pair  $(\bar{q}(1)q(2))$  should have mass  $M_W$  is particularly effective in this respect.

The  $b$  and  $\bar{b}$  jets can be identified by a secondary lepton tag (SLT), since  $b \rightarrow cW^- \rightarrow cl_2^- \bar{\nu}_l$  while  $\bar{b} \rightarrow \bar{c}W^+ \rightarrow \bar{c}l_2^+ \nu_l$ . The secondary lepton  $l^\pm$  will typically have a modest energy, say from 2 to 15 GeV for Tevatron events, and, most significant, a low  $p_T$ , say 0.2 to 1.5 GeV/c, relative to one of the jets, since the energy release for  $b \rightarrow c$  is about 3 GeV. For secondary lepton  $l_2^+$ , the associated jet will be a  $\bar{b}$ -jet; for secondary lepton  $l_2^-$ , the associated jet will be the  $b$ -jet. Since  $(W^+ \rightarrow e^+ \text{ or } \mu^+)/\text{all } W^+ \text{ decays} = 21.2(7)\%$ , SLT occurs quite often. In the decay of  $(\bar{t}t)$  systems, a single SLT must occur in 34% of the events, while a double-SLT will occur in 5% of the events. In practice, the observed rates will be lower than these since the detector efficiencies must also be taken into account; the overall efficiency reported by CDF is 20% for SLTs. However, with SLT, only 6 permutations need be considered for the other three jets.

The  $b$  and  $\bar{b}$  jets have also been identified by CDF(Abe, *et al.* 1994b) using their SVX, in which a visible decay vertex for  $b \rightarrow c$  (or  $\bar{b} \rightarrow \bar{c}$ ) has a large energy release, about 3 GeV. This contrasts with the case of a  $c$ -quark, which has a shorter lifetime, about  $0.4 \times 10^{-12}$  sec for the  $D^0$  and  $D_s^0$  states and about  $1.06 \times 10^{-12}$  sec for  $D^\pm$ , and whose dominant transition,  $c \rightarrow s$  releases much less energy, of order only 1 GeV. However, the decay vertex does not distinguish between  $b$  and  $\bar{b}$ -quark, so that a SVX-tag requires that the analysis must be carried through for both assignments, each with 6 permutations. CDF has reported that the SVX detector has an efficiency of 40%, twice that of the SLT. Multiple  $b$ -tags and  $\bar{b}$ -tags will occur; CDF(Abe, *et al.* 1994b) has already reported two events with double-SVX tags and one event with both SVX- and SLT-tags.

It is important to emphasize that each jet should be treated in an identical way, so that relative probabilities between different events and/or different interpretations can be meaningfully compared.

Our analyses of these events are summarized in Table 4, giving the values found for  $m_{pk}$  and  $LIP$  for all of the assignments which provide a fit to each event, for both possibilities, (a) that the tagged jet in the event is due to a  $b$ -quark, and (b) that the tagged jet is due to a  $\bar{b}$ -quark. This meant ignoring the charge sign for the secondary lepton for the SLT events; the implications of this sign are considered in the brief discussion we give below for each event. In most cases, there is one assignment which is more strongly favoured than the others; we then confine attention here to the fits, whether with  $b$  or  $\bar{b}$ , having the lowest  $LIP$ . Two exceptions to this remark are events 45880 and 45879, for which there are two fits and three fits, respectively, having comparable  $LIP$  values. The corresponding probability functions  $P_i(m)$  for all of these fits are plotted in Fig.8. Their spikiness is due to statistical fluctuations in our numerical evaluations of the complicated integrals involved; these curves could do with some smoothing but we have preferred to leave them as they have come out.

Four of the events have  $LIP \simeq 3.4$ , the others having the values 3.8, 5.5 and 6.3. The calculated  $LIP$  values for our 95 MC events peak at about 2.5, rising rapidly from essentially zero at  $LIP = 2.0$  to a peak value at  $LIP \simeq 2.5$  and then falling by a factor of about 10 by  $LIP = 4.5$ . The shape of the observed distribution for  $LIP$  appears qualitatively correct but with the  $LIP$  scale displaced upwards by about one unit in  $LIP$ .

Table 4. *Output from our analysis of 7 single lepton events*

(CDF's fitted values(Abe *et al.* 1994b) using a kinematical program (Dahl, *et al.* 1968) are listed below, together with their preferred jet assignment.)

	jets	LIP	$m_t$	Best Fit		CDF $m_t$	CDF $\chi^2$	
	$(b_l, q_1, q_2, b_j)$			$(x, \bar{x})$	$m(t\bar{t})$			
		CDF fitted values appear below						
Run 40758 Event 44414								
	(j4,j2,j3,j1)	3.4	$170_{-9}^{+13}$	(0.395,0.201)	507	$172 \pm 11$	<0.1	
	(j2,j3,j4,j1)	5.4	184	(0.481,0.177) (0.363,0.211)	526 498			
Run 43096 Event 47223								
	(j1,j3,j4,j2)	5.5	$162_{-4}^{+8}$	(0.521,0.139)	484	$166 \pm 11$	2.0	
	(j4,j2,j3,j1)	7.3	224	(0.529,0.152) (0.417,0.172)	511 481			
Run 43351 Event 266429								
	(j2,j1,j3,j4)	6.3	$160_{-6}^{+12}$	(0.447,0.168)	493	$158 \pm 18$	6.1	
				(0.409,0.157)	455			
Run 45610 Event 139604								
	(j2,j3,j4,j1)	3.8	$180_{-13}^{+7}$	(0.110,0.379)	367	$180 \pm 9$	5.0	
	(j1,j3,j4,j2)	5.1	112	(0.093,0.446) (0.107,0.396)	365 369			
Run 45705 Event 54765								
	(j3,j1,j2,j4)	3.4	$190_{-14}^{+11}$	(0.409,0.148)	443	$188 \pm 19$	0.4	
	(j4,j1,j2,j3)	4.95	156	(0.593,0.097) (0.388,0.135)	430 411			
Run 45879 Event 123158								
	(j2,j3,j4,j1)	3.4	$179_{-10}^{+12}$	(0.140,0.406)	423	$169 \pm 10$	2.2	
	(j2,j1,j4,j3)	3.6	180	(0.131,0.452)	438			
	(j1,j3,j4,j2)	5.7	168	(0.130,0.273) (0.129,0.420)	396 419			
Run 45880 Event 31838								
	(j1,j2,j4,j3)	3.4	$164_{-10}^{+12}$	(0.225,0.176)	358	$132 \pm 8$	1.7	
	(j2,j1,j4,j3)	3.5	$134_{-8}^{+6}$	(0.295,0.358)	358			
				(0.312,0.132)	365			

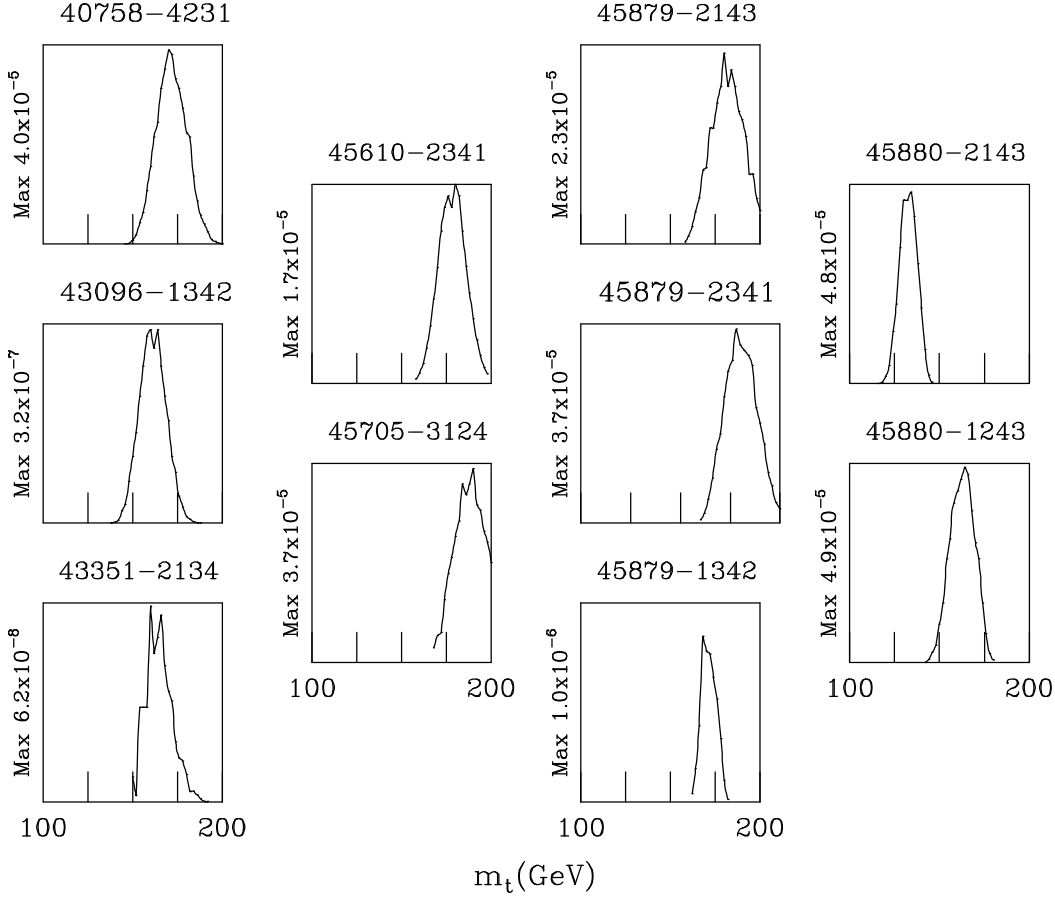


Figure 8. Plots of  $P_i(m)$  for 7 CDF unilepton events, for all promising jet assignments.

The product of the seven independent  $P_i(m)$  distributions is plotted on Fig.9, where we also show the product calculated without the events 43096 and 43351, whose  $LIP$ s exceed 5.0. These curves peak at  $172^{+2}_{-4}$  GeV, in good accord with the CDF conclusion for these events. Our general expectation that the distribution of  $m_{pk}(i)$  should consist of a fairly narrow peak appears to be the case.

We now turn to a brief discussion of the individual  $l^\pm \bar{b}b\bar{q}q$  events. The numbering of the jets, jN for N=1 to 4 for each event, is taken from CDF and given here in Table 3; the tags are specified by jet number and by type, SVX and SLT. We use the following notation for the events:  $(b_l; \bar{q}, q, \bar{b}_j)^+$  and  $(\bar{b}_l; \bar{q}, q, b_j)^-$ .  $b_l$  (or  $\bar{b}_l$ ) denotes the  $b$  (or  $\bar{b}$ ) quark (or antiquark) associated with the primary lepton  $l^+$  (or  $l^-$ ) from top (or antitop), while  $\bar{b}_j$  (or  $b_j$ ) denotes the  $\bar{b}$  (or  $b$ ) antiquark (or quark) from the decay of the associated antitop (or top) quark in the top-antitop production and decay event. The superscript  $+$  (or  $-$ ) on these two brackets gives the charge sign  $+$  (or  $-$ ) observed for the primary lepton in this event.

**40758.** This event is of type  $(\bar{b}_l; \bar{q}, q, b_j)^+$ , since the primary lepton  $e^+$  has positive charge. The SVX tag on jet j1 implies that j1 is either  $b$  or  $\bar{b}$ .

- a) For j1= $b$ , we found no fits, no matter how the other 3 jets are assigned.
- b) With j1= $\bar{b}$ , the event can only be of type  $(\bar{b}_l; \bar{q}, q, b_j)^+$ ; which jet is  $\bar{b}_l$  is to be

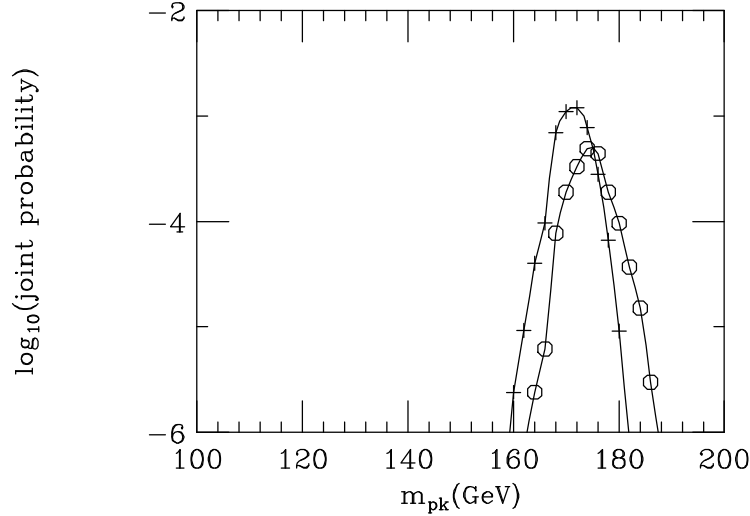


Figure 9. Logarithm of joint probability for the CDF unilepton events in Fig.8. The upper curve is for all 7 events; the lower curve has events 43096 and 43351 excluded.

determined from fits to the data, considering all 6 identifications for the other 3 quark jets. We found two fits, one corresponding to the CDF fit  $(j_4; j_3, j_2, j_1)^+$  and having  $LIP = 3.4$ , the other being  $(j_2; j_3, j_4, j_1)^+$  but having  $LIP = 5.4$ .

**43096.** This event is of type  $(\bar{b}_l; \bar{q}, q, b_j)^-$ , the primary lepton being  $e^-$ . The SVX tag on jet j1 implies that j1 is either  $b$  or  $\bar{b}$ .

a) If j1 is  $b$ , it can only be  $b_j$ ; we found only one very poor fit ( $LIP = 7.3$ ) and that was for the assignment  $(j_4; j_2, j_3, j_1)^-$ .

b) If j1 is  $\bar{b}$ , it can only be  $\bar{b}_l$ . Our only fit was  $(j_1; j_3, j_4, j_2)^-$ , as was found by CDF, here with  $LIP = 5.5$ , larger by 2 than the most probable  $LIP$  values for this batch of events.

**43351.** This event is of type  $(\bar{b}_l; \bar{q}, q, b_j)^-$ , the primary muon being  $\mu^-$ . The only fit found was  $(j_2; j_1, j_3, j_4)^-$ . There is a secondary  $\mu^-$  from j4, which suggests that j4 is  $b_j$  since the leptonic decay mode for  $b$  is  $b \rightarrow cl^- \nu$ ; this  $\mu^-$  has a  $p_T$  relative to j4 of only 0.46 GeV/c. This is all consistent with the CDF fit. So also is the fact that  $LIP = 6.3$ , which indicates a poor fit. CDF found  $\chi^2=6.1$ .

**45610.** This event is of type  $(b_l; \bar{q}, q, \bar{b}_j)^+$ , the primary muon being  $\mu^+$ . The SVX tag on jet j1 implies that j1 is either  $b$  or  $\bar{b}$ .

a) If j1 is  $b$ , it can only be  $b_l$ . We found only one fit with this assignment, given by  $(j_1; j_3, j_4, j_2)^+$  and having  $LIP = 5.1$ , marginally acceptable.

b) If j1 is  $\bar{b}$ , then j1 can only be  $\bar{b}_j$ , so we examined all 6 possibilities  $(\bar{b}_l; \bar{q}, q, j_1)^+$ , finding only one fit,  $(j_2; j_3, j_4, j_1)^+$ . It is very similar to the fit reported by CDF, and has the very acceptable  $LIP$  value of 3.8.

**45705.** This event is of type  $(\bar{b}_l; \bar{q}, q, b_j)^-$ , the primary lepton being  $e^-$ . Considering all possible assignments of the jets, we found two acceptable fits. The better fit is for  $(j_3; j_1, j_2, j_4)^-$ , with  $LIP = 3.4$ , and it is roughly comparable with the fit obtained by CDF. This fit is also in accord with the observed SLT, since this secondary lepton is an  $e^+$  with a  $p_T$  of 1.61 GeV/c relative to jet j3; the fit requires j3 to be due to a  $\bar{b}$  quark, for which we have  $\bar{b} \rightarrow \bar{c}l^+ \nu$ . Our second fit

was  $(j_4;j_1,j_2,j_3)^-$  with a poorer  $LIP$  of 5.0, but this requires  $j_3$  to be a  $b$  quark, which disagrees with the SLT, so we reject it.

**45879.** This event is of type  $(b_l;\bar{q},q,\bar{b}_j)^+$ , since the primary lepton is  $\mu^+$ . The SVX tag on jet  $j_2$  implies that  $j_2$  is either  $b$  or  $\bar{b}$ .

a) If  $j_2$  is  $b$ , then it can only be  $b_l$ . We found two fits,  $(j_2;j_3,j_4,j_1)^+$  with  $LIP = 3.4$  and  $(j_2;j_1,j_4,j_3)^+$  with  $LIP = 6$ . This event also has an SLT, a secondary  $\mu^-$  having a  $p_T$  of 0.27 GeV/c with respect to  $j_2$ .

b) If  $j_2$  is  $\bar{b}$ , then it can only be  $\bar{b}_j$ . We found one fit in this case,  $(j_1;j_3,j_4,j_2)^+$  with  $LIP = 5.3$ . This is essentially the same fit as that given by CDF. However, besides giving a less acceptable  $LIP$  value, this fit is inconsistent with the SLT  $\mu^-$  from jet  $j_2$ , since we know  $\bar{b} \rightarrow \bar{c}l^+\nu$ . For this CDF fit to be adopted, it would be necessary to accept this SLT  $\mu^-$  as a “tertiary lepton”. This would mean that the transition  $\bar{b} \rightarrow \bar{c}$  should be nonleptonic, being then followed by the tertiary decay  $\bar{c} \rightarrow \bar{s}\mu^-\nu$  which produces the observed  $\mu^-$  meson. We met a similar, but much more striking, case for the dilepton event 41540 in Sec.3, which is discussed in more detail in our Appendix below.

**45880.** This event is of type  $(\bar{b}_l;\bar{q},q,b_j)^-$ , since the primary lepton is  $e^-$ . All 24 assignments for the 4 jets were examined, and we found two fits,  $(j_1;j_2,j,j_3)^-$  for  $LIP = 3.4$  and  $(j_2;j_1,j_4,j_3)^-$  for  $LIP = 3.5$ ; the latter is similar to the fit reported by CDF. Since  $j_3$  is the  $b$  quark in both cases, they are both consistent with the observed SLT  $e^-$ , which has  $p_T=0.27$  GeV/c relative to the jet  $j_3$ .

Three of the above events are questionable. Event 43351 has  $LIP = 6.3$ , a large value corresponding to low probability. It agrees in some detail with the best fit given by CDF (Abe, *et al.* 1994b) which is however a poor fit, with  $\chi^2 = 6.1$ . This indicates that this event is most probably not an example of  $\bar{t}$ - $t$  production and decay and can be rejected with confidence. Both CDF and our analysis of event 45610 are in accord on the  $m_t$  value, but CDF report  $\chi^2 = 5.0$ , which suggests a poor fit whereas we have  $LIP = 3.8$  which is indicative of a good fit. On the other side, for event 43096, where there is good agreement in the  $m_t$  value, we have  $LIP = 5.5$ , another large value, whereas CDF find  $\chi^2 = 2.0$ , indicating a good fit. We do not yet understand these discrepancies.

## 5. Conclusions

Using QCD at tree level, we constructed by Monte Carlo methods two batches of  $p\bar{p} \rightarrow t\bar{t}$  production and decay events, for  $p\bar{p}$  center of mass energy 1.8 TeV and top mass  $m_0 = 170$  GeV, one leading to final states of the type  $l^\pm b\bar{b}$  2jets with one neutrino (or one antineutrino), and the other leading to final states of the type  $(e^+e^- \text{ or } e^\pm\mu^\mp \text{ or } \mu^+\mu^-) b\bar{b}$  with two corresponding neutrinos, using the simplest tree graph for the first step  $q\bar{q} \rightarrow t\bar{t}$ , followed by the top and antitop decay sequences. Our methods of analysis were then applied to these batches of events, in order to learn what outcome we should expect when we apply these methods to real candidate events from experiment, which may or may not be correctly interpreted as  $t\bar{t}$  production and decay events.

The outcome was remarkable. The use of the Bayesian approach led us to a probability distribution for the mass value  $m(i)$  for each event  $i$ , and thence to a distribution of the peak mass values  $m_{pk}(i)$  for all  $i$ , separately for the two batches. The final distributions for the two batches proved to be unexpectedly

different, that for the unilepton events being sharp and peaking only several GeV below the input mass  $m_0$ , while that for the dilepton- $b\bar{b}$ (jets) was very broad and strongly asymmetrical. With  $m_0 = 170$  GeV, the latter distribution has a mean mass of 162.0, its median being about 165.0 GeV. This means that half of the dilepton events analysed lead to peak values lying at or below 165 GeV. In our earlier analyses of real events (Dalitz & Goldstein 1995), we had already noticed this tendency for dilepton mass values to lie lower in mass than those for the unilepton mass values and commented upon it more than once. Now we see that this behaviour was to have been expected.

We made similar calculations for batches constructed for input mass  $m_0 = 140$  GeV, and some of the corresponding distributions have been recorded in the main text. They have some educational value, although being no doubt academic.

Three more detailed comments follow:

- i) Our analysis of the seven  $l^\pm 4j$  events now known is in general accord with the CDF-analysis, especially with their mass estimate of about 175 GeV. Two of the events have very low likelihoods in our analysis, while two of them have relatively large  $\chi^2$  in the CDF analysis, one event being rejected by both; four events stand firm in both analyses. The three events rejected may be due to background such as that originating from the processes  $W^\pm + 4jets$  with  $W^\pm \rightarrow l^\pm$ , as discussed by Berends, *et al.* 1991, although those authors show that tagging a single  $b(\bar{b})$  quark should significantly reduce that background. Their calculations indicate a suppression of background by about  $10^{-2}$  when both  $b$  and  $\bar{b}$  are tagged. More estimates from other mechanisms involving b-quarks need to be considered quantitatively, within the framework of our analysis procedure.
- (ii) We have not paid attention to the relative rates for  $l^\pm 4jets$  and  $(e^+e^-$  or  $e^\pm\mu^\mp$  or  $\mu^+\mu^-)2jets$  events, and this is an important problem for the future. Accepting that four b-tagged events of the former class have been observed, we need to calculate the expected number of events of the latter class. This is a complicated calculation, which is sensitive to the precise cuts which are imposed and which we do not attempt to carry out here. The efficiencies depend on whether the lepton in question is an electron or a muon. The nature of the identification given by tagging is different for SVX and SLT. SVX does not distinguish  $b$  from  $\bar{b}$ , since it determines only the location of the secondary vertex, while SLT does not give the location of the vertex but does distinguish between  $b$  and  $\bar{b}$ . Since the c-quark decay lifetime is shorter than that for the b-quark, there should frequently be seen a tertiary vertex arising from c decay, not far from a secondary b-vertex.
- iii) Finally, the peak masses  $m_t$  determined empirically appear to be somewhat lower for  $e^\pm\mu^\mp 2jet$  events, on average, than for  $l^\pm 4jet$  events, in accord with the qualitative expectations from our QCD model and its numerical evaluation. It will be of interest to watch how the empirical data turn out in future, after the Main Injector comes into operation at Fermilab. As things now stand, there is no clear discrepancy between our analyses of these two classes of events.

The authors are grateful to J. Ohnemus for supplying a copy of an efficient Monte Carlo code with importance sampling and to P. Sphicas, Tony Smith, K. Kondo, K. Sliwa and D0 group members for many useful conversations. G.R.G. thanks the U.S. Department of Energy for partial support of this research (DE-FG-02-92ER40702), and Prof. John Negele for hospitality at the MIT Center for Theoretical Physics during a sabbatical leave when an earlier version of this work was begun. We appreciate the hospitality of Prof. D. Sherrington at the Department of Theoretical Physics, Oxford.



### Appendix A. Appendix. Secondary and tertiary leptons.

The CDF dilepton event 41540 has a unique interpretation when analysed as  $\mu^+e^-j(1)j(2)$ ,  $j(1)$  being identified as the  $b$ -jet and  $j(2)$  as the  $\bar{b}$ -jet (see Table 1). The jet  $j(3)$  is close to the initial direction, being most probably due to gluon bremsstrahlung. The event has a third lepton, a “slow”  $\mu^+$  of energy 8.9 GeV. The routine choice of associating this lepton with the  $\bar{b}$  jet is not convincing since its largest momentum component,  $p_x(\mu^+) = 8.7$  GeV, is oppositely directed to the largest component of the jet 2 momentum,  $p_x = -50.0$  GeV. It is much more plausible that the “slow”  $\mu^+$  is associated with jet 1, since its momentum is almost parallel with the momentum of jet 1, and in the same direction; its momentum  $p_\perp$ , transverse to jet 1 is only about 0.6 GeV/c.

The sequence of quark processes which lead to the emission of a tertiary  $\mu^+$  lepton, (A2) with, and (A3) without, a secondary  $\mu^-$  lepton, are as follows:

$$t \rightarrow b + W^+ \qquad W^+ \rightarrow \mu^+ + \nu_\mu, \qquad (\text{A } 1)$$

$$b \rightarrow c + W^- \qquad W^- \rightarrow \mu^- + \bar{\nu}_\mu \qquad (\text{A } 2)$$

$$\text{or} \qquad W^- \rightarrow \text{hadrons}(\bar{u}d + \bar{c}s), \qquad (\text{A } 3)$$

$$c \rightarrow s + W^+ \qquad W^+ \rightarrow \mu^+ + \nu_\mu, \qquad (\text{A } 4)$$

the  $W$ 's in (A 2), (A 3) and (A 4) being necessarily virtual, of course. The net process for the event 41540 would be the consequence of (A 1),(A 3) and (A 4), thus:

$$t \rightarrow \text{hadrons} + \mu^+(\text{fast}) + \mu^+(\text{slow}) + \text{neutrinos}. \qquad (\text{A } 5)$$

To orient ourselves concerning the final states, we have made some simple model calculations for the momentum distributions for a secondary lepton  $l_2$ , or for a tertiary lepton  $l_3$ , appropriate for an initial  $b$ -jet with momentum about 130 GeV/c. We adopted the fragmentation functions of Peterson *et al.* (1983), with the parameter  $\epsilon_Q = (0.49)/m_Q^2$  GeV<sup>-2</sup>, where  $m_Q$  denotes the appropriate heavy quark mass. In the first step, the  $b$ -quark generally undergoes hadronization to a final ground state meson  $B_u^-$ ,  $B_d^0$  or  $B_s^0$  with spin-parity  $0^-$ , together with some number of light mesons; we neglect explicit mention of hadronization to  $\Lambda_b$  baryons, since such final states contribute much less and do not affect the over-all conclusions. Using the standard model expression for the momentum distribution of the lepton resulting from  $b \rightarrow cl_2\nu_l$  in the B-meson rest frame, we obtain the  $l_2^-$  momentum distribution in the lab frame by integrating this distribution over the B-momentum distribution given by the fragmentation function. The resulting energy distribution for secondary leptons is given in Fig.10(a). We note that these energies run up to very large values. The mean  $l_2^-$  energy is  $\approx 33$  GeV/c and 50% of the leptons have energy greater than 29 GeV. The distribution for  $p_\perp$ , the secondary muon momentum transverse to the B-momentum, is given in Fig.11(a), although we must note that the B-momentum is affected by the gluons and light mesons emitted so that it differs a little from the  $b$ -jet axis observed. The most probable value for  $p_\perp(l_2)$  is 1.4 GeV/c; its median value is 1.35 GeV/c. For 90% of the secondary leptons,  $p_\perp(l_2)$  exceeds 0.6 GeV/c; 70% of them have  $p_\perp(l_2) \geq 1$  GeV/c. For tertiary leptons, we must first carry out the same calculation for the lab momentum distribution of the  $c$ -quarks from the  $b$ -jet. Naturally, this

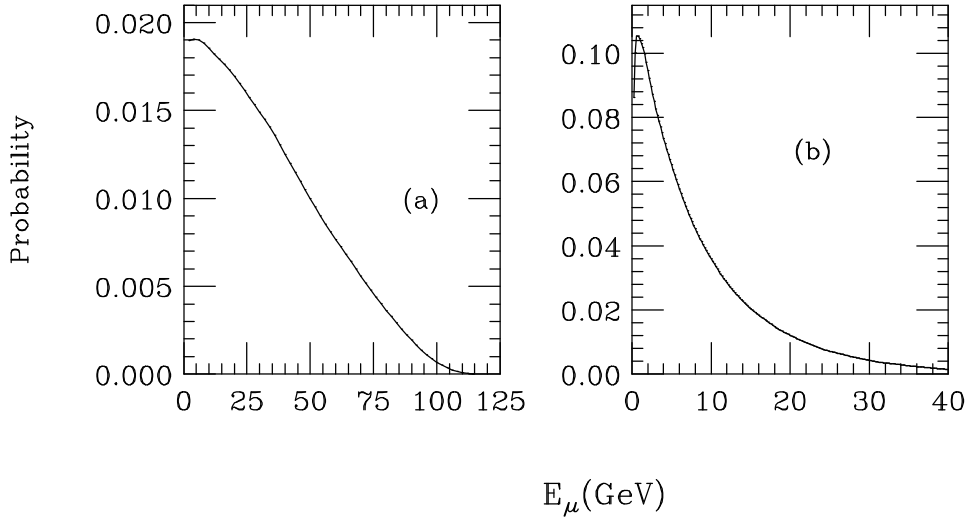


Figure 10. (a) The energy distribution in the Lab. frame, for the secondary leptons resulting from the decay  $b \rightarrow c + l^- + \nu_l$ , for a b-quark jet of initial energy 130 GeV; (b) The energy distribution in the Lab. frame, for tertiary leptons resulting from the decay  $c \rightarrow s + l^+ + \nu_l$ , for a b-quark jet of initial energy 130 GeV.

distribution is quite different from that for the secondary leptons, because of the large mass value for the c-quark. The lab energy distribution for the  $l_3^+$  lepton from  $c \rightarrow sl_3^+ \nu_l$  decay is then obtained by integrating the latter, as given by the standard model, over the fragmentation function for the ground state  $0^-$  ( $D_u, D_d$  and  $D_s$ )-mesons from the c-jet distribution just calculated. The resulting energy distribution for the  $l_3^+$  lepton is shown in Fig.10(b). We note that these energies are much less than those for secondary leptons but their distribution is very asymmetric; their peak value is  $\approx 0.5$  GeV, while their median value is  $\approx 5$  GeV. Above 1 GeV, the distribution falls gradually with increasing energy  $E(l_3)$ , by a factor of 3 from 5 to 15 GeV, and then faster beyond; 25% of the tertiary leptons have  $E(l_3) \geq 10$  GeV, but only 9% have energies exceeding 15 GeV. The distribution for the transverse momentum  $p_\perp(l_3)$  is shown on Fig.11(b). It peaks at 0.35 GeV/c and is a little asymmetric; about 30% of the events have  $p_\perp(l_3) \geq 0.6$  GeV/c, about 5% have  $p_\perp(l_3) \geq 1.0$  GeV/c.

We now return to the consideration of event 41540. That the “slow”  $\mu^+$  lepton is associated with jet 1 is supported by a close examination of the event shown in Fig.10 and Table VII of the CDF paper (Abe *et al.* 1994b). There is a displaced vertex shown in the SVX detector, at  $\bar{r} = 0.33$  cm from the origin of the event. Comparison of the  $\phi$  distribution in their Fig.10(b) with the entry in their Table VII shows us that the secondary vertex shown is associated with the b-jet (jet 1). We are not told where the 8.9 GeV/c  $\mu^+$  emerged. The two most immediate possibilities are:

(T<sub>1</sub>) the displaced vertex is a non-leptonic b-decay, the ratio  $\bar{r}/\bar{d}_B$  being 0.26, where  $\bar{d}_B = \gamma_B c \tau_B$  is the mean distance of travel by the b-quark before decay,  $\gamma_B m_B = 131$  GeV/c, and  $\tau_B$  being the B-meson lifetime. The resulting c-quark then undergoes decay  $c \rightarrow s \mu^+ \nu_\mu$ , leading to a “slow”  $\mu^+$  which is tertiary. The chance that this c-decay occurs outside the SVX region is about  $e^{-((d-\bar{d}_B)/\bar{d}_D)}$  where  $d = 0.5$  cm and  $\bar{d}_D = \gamma_D c \tau_D$ . Taking  $\gamma_D$  to have value about the same

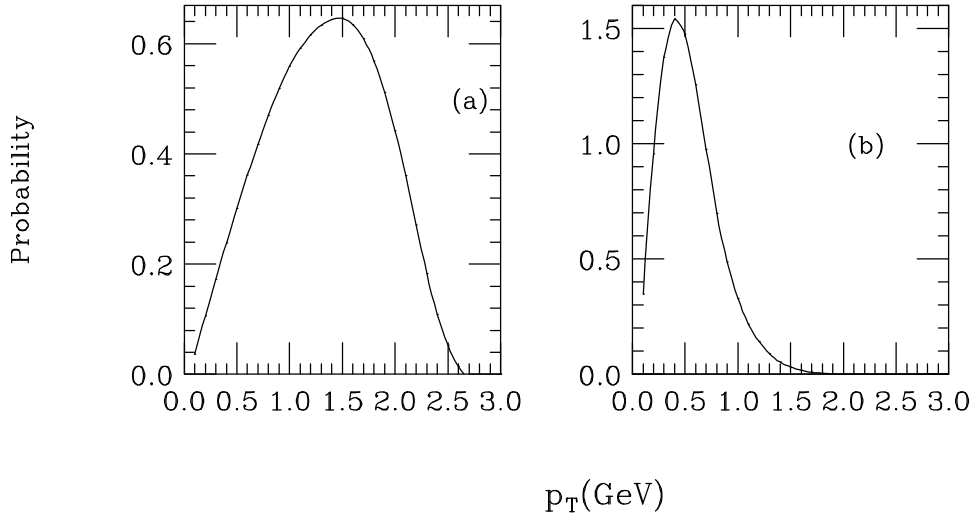


Figure 11. (a) The distribution of the momentum transverse to the b-jet axis, for secondary leptons resulting from the decay  $b \rightarrow c + l^- + \nu_l$ , for a b-quark jet of initial energy 130 GeV; (b) The distribution of the momentum transverse to the b-jet axis, for tertiary leptons resulting from the decay  $c \rightarrow s + l^+ + \nu_l$ , for a b-quark jet of initial energy 130 GeV.

as  $\gamma_B$ , we then have  $\bar{d}_D$  about 0.37 cm, which gives the chance of the c-quark escaping without detection to be about 40%.

(T<sub>2</sub>) The vertex observed is a tertiary decay, the “slow”  $\mu^+$  being one of the tracks observed (whether or not it is identified) and coming from the transition  $c \rightarrow s\mu^+\nu_\mu$ . The only question is “where is the b-quark decay vertex?” To give rise to what is observed, there should then be a b non-leptonic vertex between the origin and the displaced vertex, but perhaps so close to the tertiary vertex, in view of the rapidity of c-decay relative to b-decay, that it may be difficult to separate the two vertices. Also, in this case, there should necessarily be a “slow”  $\mu^+$  emitted from the displaced vertex, although there is no clear statement identifying this  $\mu^+$  in the SVX data. It is difficult to estimate the probability for this outcome, without more detailed information. A much closer examination of the SVX data on this event is needed.

Such tertiary leptons will not be rare. The branching fraction (BF) for all leptonic modes is known (Particle Data Group 1996) to be about 21.0(4)% for the b quark and about 23(3)%, on average, for the c quark, assuming that the configurations  $(\bar{u}c)$ ,  $(\bar{d}c)$  and  $(\bar{s}c)$  are produced equally often. (For the  $D$  mesons, the BF’s are 34.4(38)% for  $D^+$  and 17.7(24)% for  $D^0$ . From their known lifetimes their leptonic decay rates are therefore  $3.3(4) \times 10^{11} \text{ s}^{-1}$  and  $4.3(7) \times 10^{11} \text{ s}^{-1}$ , respectively, in fair agreement with each other. The well known inequality between their total decay rates (and therefore between their leptonic BF’s) is due to a suppression of the non-leptonic decay modes of  $D^+$  relative to those for the  $D^0$ . However, it is leptonic BF’s which are relevant for discussing the possibilities for tertiary leptons. The leptonic BF’s are not known for  $D_s^+$ , only the upper limit,  $< 20\%$ , but its total lifetime is within three standard deviations of that for  $D^0$ .) Neglecting corrections for the efficiencies for detecting SLT’s, generally stated to be about 30% but which may be substantially lower than this for the detection of tertiary leptons, we may estimate that the frequency of tertiary lep-

tons without any secondary lepton is comparable with the frequency of secondary leptons without any tertiary lepton.

However, there is an alternative interpretation possible for the “slow”  $\mu^+$ :

(S<sub>d</sub> or S<sub>s</sub>) The hadronization of the b-jet may lead to a charged  $B^-$  meson or to a neutral meson,  $B_d^0$  or  $B_s^0$ . In the latter two cases, the meson may undergo the process of  $(B_d^0, \bar{B}_d^0)$  mixing or  $(B_s^0, \bar{B}_s^0)$  mixing, and can then emit a  $\mu^+$  lepton from the secondary process  $\bar{b} \rightarrow \bar{c}\mu^+\nu_\mu$ , since this will be possible from the  $\bar{b}$ -quark in the  $\bar{B}_d^0$  or  $\bar{B}_s^0$  components of the final mixed  $(\bar{B}^0, B^0)$ -meson state. From data on b-jet development following the much studied process  $Z^0 \rightarrow b\bar{b}$ , it is known that the secondary  $\mu^+$ 's from this source have an intensity 13% of the total from the secondary  $(\mu^+ + \mu^-)$  leptons from the initial b-quark. These secondary  $\mu^+$ 's from mixing will have the same energy spectrum as the  $\mu^-$  secondary leptons from all three kinds of final B-meson, which we have estimated from our model calculation to have the form shown in Fig.10(a), a spectrum much harder than our estimate for the tertiary  $\mu^+$  spectrum, given in Fig.10(b).

We may now our calculated probability curves to assess the relative likelihood of the two hypotheses, T and S, just discussed above.

(S)  $b \rightarrow \bar{b} \rightarrow \bar{c}l^+$  and  $b \rightarrow cl^-$ .

As noted above, it is known (Particle Data Group 1996) that the rate for  $l^+$  is  $\epsilon = 0.13$  times that for  $(l^+ + l^-)$  when the sum is over  $B_d^0$  and  $B_s^0$  mesons. We denote the distribution of the final secondary lepton by  $P_2(E_l)$ , shown in Fig.10(a), and the distribution of the secondary lepton momentum transverse to the b-jet axis by  $Q_2(p_{l\perp})$ , shown in Fig.11(a). From the Particle Data Group 1996, we take  $B_{bl} = 0.207$  for the branching fraction  $(b \rightarrow \text{all } l^\pm)/(\text{all } b \text{ decays})$ . The net rate for  $l^+$ , occuring as secondary leptons, is given by

$$R_S = \epsilon \cdot B_{bl} \cdot P_2(E_l) \cdot Q_2(p_{l\perp}). \quad (\text{A } 6)$$

per initial b quark.

(T)  $b \rightarrow c \rightarrow l^+$ , with no secondary lepton.

Here we ignore the SVX detector, i.e. we do not require the second decay to be visible within it. We take  $B_{cl} = 0.34$  (Particle Data Group 1996) as the branching fraction  $(c \rightarrow \text{all } l^\pm)/(\text{all } c \text{ decays})$ . The net rate for  $l^+$  is now,

$$R_T = (1 - B_{bl}) \cdot B_{cl} \cdot P_3(E_l) \cdot Q_3(p_{l\perp}). \quad (\text{A } 7)$$

per initial b quark.

For the event of interest, we have  $E_\mu = 8.9$  GeV and  $p_{\mu\perp} = 0.60$  GeV/c. The interpretation S that the “slow”  $\mu^+$  lepton is due to  $(\bar{B}^0, B^0)$  mixing gives the rate per initial b quark as

$$R_S = 0.22 \times 0.13 \times 0.018 \times 0.36 = 4.4 \times 10^{-4}. \quad (\text{A } 8)$$

With the tertiary interpretation T, we have the rate

$$R_T = 0.78 \times 0.33 \times 0.035 \times 1.24 = 1.12 \times 10^{-2}. \quad (\text{A } 9)$$

Hence the calculations with our simple model for the decay sequences  $b \rightarrow cl^+\nu$  and  $b \rightarrow c \rightarrow sl^+\nu$  indicate that the likelihood that this  $\mu^+$  is tertiary relative to the likelihood that it is secondary - but results from  $(\bar{B}^0, B^0)$  mixing - is 25:1. The main factor depressing the rate  $R_S$  is the low value for  $\epsilon$ ; surprisingly, the observed values for  $E_l$  and  $p_{l\perp}$  do not distinguish clearly between the possibilities S and T.

Table 5. *Events available having a secondary or tertiary lepton*  
(Energies in GeV, momenta in GeV/c. Bracket denotes possible tertiary lepton.)

Event	43351	45705	45879	45880	41540
$E_{1l}$	24.7	70.0	54.0	26.1	48.2
$E_{bj}$	39.0	70.7	96.7	46.5	131.8
$E_{2l}$	2.37	14.28	13.58	2.80	(8.9)
$E_{2l}/(E_{2l} + E_{bj})$	5.7%	16.0%	12.6%	5.7%	(6.8%)
$p_{l\perp}$	0.46	1.615	0.27	0.27	0.60
$p_{l\perp}/(E_{2l} + E_{bj})$	1.1%	1.45%	0.25%	0.55%	(0.43%)

It is of interest to compare event 41540 with those SLT  $l4$ jets events reported by CDF, which can be assigned uniquely and kinematically to secondary lepton emission. These are the events where the lepton charge has sign in accord with the decay  $b \rightarrow cl^-\bar{\nu}$  (or  $\bar{b} \rightarrow \bar{c}l^+\nu$ , for events which stem from  $\bar{t}$  production and decay). We note that the primary lepton energies  $E_{1l}$  have a reasonable spread of energies, from 24.7 to 117.3 GeV, as shown in Table 3. The two energies  $E_{1l}$  in the dilepton events lie at energies in the range  $\approx 30-70$  GeV. The four “slow” leptons available have energies  $E_{2l}$  which range from 2.4 to 14.3 GeV, while the “slow”  $\mu^+$  energy in event 41540 lies in the middle of this range. The same holds for its  $p_{l\perp}$  value. Since the b-jet energy in this event has a surprisingly large value,  $(E_{bj} + E(SLT))$  being  $\approx 141$  GeV (overlooking the unknown neutrino energy resulting from this b-decay), we might look instead at the weighted energies  $E(SLT)/(E(SLT) + E_{bj})$  and transverse momenta  $p_{l\perp}/(E(SLT) + E_{bj})$ , listed in Table 5. Even then, their values for 41540 still lie within the ranges obtained for these parameters from the four  $l4$ jets events. None of these numbers mark out this SLT event as being obviously different from the other SLT events, except for the charge sign for the “slow”  $\mu^+$  and the magnitude of the ratio  $R_T/R_S$  discussed above.

Finally, we must compare these four SLT  $l4$ jets events with the calculated spectra for our simple  $(b \rightarrow cl^-\bar{\nu}, \bar{b} \rightarrow \bar{c}l^+\nu)$  model. Fig. 10(a) shows that the median value predicted for secondary lepton energy  $E_{2l}$  lies at  $\approx 30$  GeV for the dilepton event 41540, with 130 GeV for jet 1 lab energy  $E_{bj}$ . The four SLT events have lower b-jet energies, ranging from 39 to 97 GeV. This does not effect the  $p_{l\perp}$  spectrum, but it alters the  $E_{2l}$  spectra. For each event the energy spectrum will depend on the boost from the decaying B rest frame to the lab frame (in which the B meson is a fragment of the b-jet). For the event with the lowest associated b-jet energy, event 43351, the corresponding spectrum will have a median of about 9 GeV, compared to the measured  $E_{2l} = 2.37$  GeV. The median energy grows roughly linearly with jet energy, so the secondary lepton in each of these four events have generally lower energy,  $E_{2l}$ , than the predicted median. Three of these SLT events have  $p_{l\perp}$  values that lie below 0.5 GeV/c, whereas our model predicts its median to be  $\approx 1.35$  GeV/c. The accord of these data with our

calculations is neither striking nor unfavourable. It may be that the cuts made on the data by the experimenters, aimed at picking out any background events, have a much larger effect on the predicted curves in Figs.10 and 11 than we have anticipated.

Double-tagging, the combination of the secondary vertex detector (SVX) and the observation of secondary leptons (SLT) together should provide a powerful means for interpretation of the nature of individual events, without a full dynamical analysis (which would at best be possible only rarely). The above analysis of event 41540 illustrates this point quite strongly.

### References

- Abachi, S. *et al.* 1995 Observation of top quark production in  $\bar{p}p$  collisions with the collider detector at Fermilab. *Phys. Rev. Lett.* **74**, 2632-2637.
- Abachi, S. *et al.* 1997 Direct measurement of top quark mass. *Phys. Rev. Lett.* **79**, 1197-1202.
- Abbott, B. *et al.* 1997 Measurement of the top quark mass using dilepton events. Preprint no. Fermilab-Pub-97/172<sub>E</sub> and hep-ex/9706014, Fermilab, Batavia, IL, USA.
- Abe, F. *et al.* 1990 Search for new heavy quarks in electron-muon events at the Fermilab Tevatron Collider. *Phys. Rev. Lett.* **64**, 147-151.
- Abe, F. *et al.* 1994a Evidence for top quark production in  $\bar{p}p$  collisions at  $\sqrt{s} = 1.8$  TeV. *Phys. Rev. Lett.* **73**, 225-231.
- Abe, F. *et al.* 1994b Evidence for top quark production in  $\bar{p}p$  collisions at  $\sqrt{s} = 1.8$  TeV. *Phys. Rev.* **D50**, 2966-3026.
- Abe, F. *et al.* 1995a Observation of the top quark. *Phys. Rev. Lett.* **74**, 2626-2631.
- Abe, F. *et al.* 1995b Kinematic evidence for top quark pair production in W+multijet events in  $p\bar{p}$  collisions at  $\sqrt{s} = 1.8$  TeV. *Phys. Rev.* **D51**, 4623-4637.
- Abe, F. *et al.* 1997 First observation of all hadronic decay of top-antitop pairs. *Phys. Rev. Lett.* **79**, 1992-1997.
- Barger, V.D. & Phillips, R.J.N. 1987 *Collider Physics* pp. 319-330. Redwood City, Calif.: Addison-Wesley.
- Barger, V.D., Han, T., Zeppenfeld, D. & Ohnemus, J. 1990 Pair production of  $W^\pm$ ,  $\gamma$ , and Z in association with jets. *Phys. Rev.* **D41**, 2782-2794.
- Benlloch, J.M., Wainer, N. & Giele, W.T. 1993 On the search for the top quark in the hadronic decay channel. *Phys. Rev.* **D48**, 5226-5232.
- Berends, F.A. *et al.* 1991 On the production of a W and jets at hadron colliders. *Nucl. Phys.* **B357**, 32-64.
- Dahl, O., Day, T., Solmitz, F. & Gould, N. 1968 Group A programming note P-126. Report, Lawrence Berkeley Laboratory, University of California at Berkeley, USA.
- Dalitz, R.H. & Goldstein, G.R. 1992a The analysis of top-antitop production and dilepton decay events and the top quark mass. *Phys. Lett.* **B287**, 225-230.
- Dalitz, R.H. & Goldstein, G.R. 1992b The decay and polarization properties of the top quark. *Phys. Rev.* **D45**, 1531-1543.
- Dalitz, R.H. & Goldstein, G.R. 1994 Where is top? *Int. J. Mod. Phys.* **A9**, 635-666.
- Dalitz, R.H. & Goldstein, G.R. 1995 Top mass analysis of the reported top-antitop production and decay events. Preprint no. hep-ph/9506232, Tufts University, Medford, MA, USA.
- Giromini, P. 1997 Top physics. In *Proc. 18th Intl. Conf. on Lepton-Photon Interactions, Hamburg, Germany, 28 July 1997*, to be published.
- Goldstein, G.R., Sliwa, K. & Dalitz, R.H. 1993 Observing top-quark production at the Fermilab Tevatron. *Phys. Rev.* **D47**, 967-972.
- Han, T. & Parke, S. 1993 Heavy top-quark searches in the dilepton mode at the Fermilab Tevatron. *Phys. Rev. Lett.* **71**, 1494-1497.

- Kondo, K. 1988 Dynamical likelihood method for reconstruction of events with missing momentum. I. Method and toy models. *J. Phys. Soc. Japan* **57**, 4126-4140.
- Kondo, K. 1991 Dynamical likelihood method for reconstruction of events with missing momentum. II. Mass spectra for  $2 \rightarrow 2$  processes. *J. Phys. Soc. Japan* **60**, 836-844.
- Kondo, K., Chikamatsu, T. & Kim, S.H. 1993 Dynamical likelihood method for reconstruction of events with missing momentum. III. Analysis of a CDF high  $p_T$   $e\mu$  event as  $t\bar{t}$  production. *J. Phys. Soc. Japan* **62**, 1177-1181.
- Kruse, M.C. 1996 Observation of top quark pair production in the dilepton channel for proton-antiproton collisions at 1.8 TeV. Ph.D. thesis, Purdue University, Lafayette, IN, USA.
- Particle Data Group 1996 Review of particle properties. *Phys. Rev.* **D54**, 1-720.
- Peterson, C. *et al.* 1983 Scaling violations in inclusive  $e^+e^-$  annihilation spectra. *Phys. Rev.* **D27**, 105-111.
- Sliwa, K. 1991 Search for top quark at Fermilab Collider. In *Proc. XXV Intl. Symposium on Heavy Flavor Physics, Orsay, France*, (ed. M. Davier & G. Womser). Gif-sur-Yvette, France: Edition Frontieres, pp. 567-577.
- Varnes, E.W. 1997 Measurement of the top quark mass. Ph.D. thesis, University of California at Berkeley, CA, USA.

*Received*